Rad53 phosphorylation of Rdh54 regulates the lifetime of homologous recombination intermediates

Jingyi Hu[1], Bryan Ferlez[1], Jennifer Dau[1], and J. Brooks Crickard [1#]

[1.] Department of Molecular Biology and Genetics, Cornell University, Ithaca, NY 14853, USA
#To whom the correspondence should be addressed: jbc287@cornell.edu

Words: 6028
Characters: 38,917
Keywords: Homologous recombination, Rad53, Rdh54, DNA repair

Abstract
Rdh54 is a conserved DNA translocase that participates in homologous recombination (HR), DNA checkpoint adaptation, and chromosome segregation. *Saccharomyces cerevisiae* Rdh54 is a known target of the Mec1/Rad53 signaling axis, which globally protects genome integrity during DNA metabolism. While phosphorylation of DNA repair proteins by Mec1/Rad53 is critical for HR progression little is known about how specific post translational modifications alter HR reactions. Phosphorylation of Rdh54 is linked to protection of genomic integrity but the consequences of modification remain poorly understood. Here, we demonstrate that phosphorylation of the Rdh54 C-terminus by the effector kinase Rad53 down regulates Rdh54 activity resulting in a 50% decrease in translocation velocity on dsDNA as revealed by single molecule imaging. Genetic assays reveal that loss of phosphorylation reduces interhomolog gene conversion, increases break induced replication, and decreases crossover outcomes. Our data highlight Rad53 as a key regulator of HR intermediates through activation and attenuation of Rdh54 motor function.

Introduction
DNA double strand breaks (DSBs) are a dangerous type of DNA lesion that if unrepaired result in cell death or loss of genomic integrity (Scully *et al*, 2019). DSBs result from normal DNA metabolism, and from exposure to mutagens within the environment (Mehta & Haber, 2014; Scully *et al.*, 2019; Wyman & Kanaar, 2006). This makes double strand break repair (DSBR) critical for the maintenance of genomic integrity. DSBR is a multi-tier decision making process in which multiple pathways can be used to repair the break depending on the phase of the cell cycle. The two primary DSBR pathways are non-homologous end joining (NHEJ) and homologous recombination (HR) (Scully *et al.*, 2019). HR is a template based DSBR pathway that is primarily active during S/G2 phase of the cell cycle and meiosis (Filippo *et al*, 2008; Hunter, 2015; Symington *et al*, 2014; Szostak *et al*, 1983; Wyman & Kanaar, 2006). Nested within HR is a secondary decision tree that ensures HR will be completed through one of several competing pathways outlined below (Scully *et al.*, 2019). These pathways are dependent on key intermediates including the selection of a donor DNA template (Bell & Kowalczykowski, 2016; Greene, 2016; Haber, 2018; Kowalczykowski, 2015; Renkawitz *et al*, 2014; Renkawitz *et al*, 2013), and the location and timing of second end capture (Mazloum & Holloman, 2009; McIlwraith & West, 2008; Mehta *et al*, 2017; Nimonkar *et al*, 2009; Pham *et al*, 2021).

In eukaryotes coordination of template selection is carried out by the recombinase Rad51 (Filippo *et al.*, 2008; Qi *et al*, 2015; Xu *et al*, 2017), which catalyzes the alignment of ssDNA (recipient

DNA) from upstream of the DSB to a matching dsDNA (donor DNA) elsewhere in the genome in a process called the homology search. In *Saccharomyces cerevisiae*, Rad51 is aided in alignment of recipient and donor DNA by several accessory factors including Rad52, Rad54, Rdh54, and Rad55/57 (Chi *et al*, 2006; Crickard *et al*, 2020a; Crickard *et al*, 2020b; Lisby *et al*, 2004; Lisby & Rothstein, 2015; Mazin *et al*, 2000; Petukhova *et al*, 2000; Piazza *et al*, 2019; Roy *et al*, 2021; Sugawara *et al*, 2003; Tavares *et al*, 2019). In mitotic HR, the sister chromatid is the primary template used for repair and results in the highest fidelity outcome (Kadyk & Hartwell, 1992; Piazza *et al*, 2021). However, in rare cases the homologous chromosome is used as the template for repair. When the homologous chromosome is used as the template there is potential for gene conversion (Chen *et al*, 2007), which can result in a loss-of-heterozygosity (LOH) (Hügel & Wernert, 1999; Moynahan & Jasin, 1997; Nichols *et al*, 2020; Ryland *et al*, 2015). Therefore, template selection becomes the first key choice during the HR reaction.

After template selection, strand invasion intermediates known as the displacement loop (D-loop) form (Piazza & Heyer, 2019; Piazza *et al.*, 2019). As this intermediate matures a second major decision occurs when the second end of the broken recipient DNA is captured. If second end capture occurs outside of the D-loop there is no additional exchange of genetic material. This sub-pathway is known as synthesis-dependent strand annealing (SDSA) (Chen *et al.*, 2007). If second end capture occurs within the D-loop then this leads to the formation of a double Holliday junction (dHJ) and the classical DSBR pathway (Bzymek *et al*, 2010; Szostak *et al.*, 1983). The DSBR also creates the potential for another decision during HR, the resolution of dHJs by crossover (CO) or non-crossover outcomes (NCO) (Szostak *et al.*, 1983). COs result in further exchange of DNA between donor and recipient DNA molecules. The last outcome associated with second end capture is when the second end is not found. This results in the initiation of break-induced replication (BIR) (Kockler *et al*, 2021; Kramara *et al*, 2018; Malkova & Ira, 2013; Pham *et al.*, 2021; Wu & Malkova, 2021). BIR is a highly mutagenic DNA repair outcome (Kockler *et al.*, 2021).

Decisions to use each of these pathways are influenced by the timing of each step, which is under the regulation of DNA damage kinases (Waterman *et al*, 2020). These kinases also play established roles in slowing cell cycle progression. As a result, their activation provides more time for the execution of DNA repair before cell division and reduce the passage of damaged DNA (Waterman *et al.*, 2020). In *S. cerevisiae*, the sensor kinase Mec1 plays a predominant role in activation of damage signaling kinases (Navadgi-Patil & Burgers, 2011), with its major downstream target being the effector kinase Rad53 (Chen & Zhou, 2009; Lee *et al*, 2003; Mordes *et al*, 2008; Navadgi-Patil & Burgers, 2011). Rad53 phosphorylates proteins within the HR pathway (Sanford *et al*, 2021; Waterman *et al.*, 2020), at the replication fork (Alcasabas *et al*, 2001; Bacal *et al*, 2018; Devbhandari & Remus, 2020), and at the kinetochore where it regulates chromosome division (Agarwal *et al*, 2003; Krishnan *et al*, 2004; Palou *et al*, 2017; Schwartz *et al*, 2003). These kinases are believed to influence DNA repair pathway choice during DSBR. Failure to repair a DSB in a defined period can result in cell death, or checkpoint adaptation (Lee *et al*, 2001; Swift & Golsteyn, 2016). Checkpoint adaptation results in division despite damaged DNA and is designed to keep the cell growing and to repair the damaged DNA in G1 of the next cell cycle (Lee & Petes, 2010). Hyperactivation of adaptation is highly mutagenic during cancer tumor growth (Coutelier *et al*, 2018; Kumar *et al*, 2021).

Rdh54 is a DNA motor protein that uses the power of ATP hydrolysis to physically move along dsDNA, and directly interacts with Rad51 at HR intermediates (Chi *et al.*, 2006; Crickard *et al.*, 2020a; Nimonkar *et al*, 2007; Prasad *et al*, 2007). Rdh54 has been shown to stabilize Rad51 bound to ssDNA and D-loops, and to disrupt Rad51 bound to dsDNA (Keymakh *et al*, 2022; Meir *et al*, 2022; Shah *et al*, 2010; Shah *et al*, 2020). Several studies have implicated Rdh54 in biasing outcomes at each one of the major decision steps during HR. These include regulating CO/NCO outcomes (Piazza *et al.*, 2019; Shinohara *et al*, 1997), BIR outcomes (Keymakh *et al.*, 2022), interhomolog gene conversion (Klein, 1997; Shinohara *et al.*, 1997), checkpoint adaptation (Ferrari *et al*, 2013), and chromosome segregation (Sharp *et al*, 2018). Importantly, apart from checkpoint adaptation, Rdh54 is not required for completion of these pathways, and instead appears to only influence HR choices indirectly. It has also been suggested that Rdh54 activity is context dependent. Rdh54 is a target of the Mec1/Rad53 signaling axis (Ferrari *et al.*, 2013), but it is unknown if phosphorylation of Rdh54 may provide that context.

Here we have investigated the role of Rdh54 phosphorylation in regulation of HR activity. We find that Rdh54 is a direct target of the effector kinase Rad53. Phosphorylation of Rdh54 at a specific amino acid residue results in increased enzymatic cooperativity between adjacent Rdh54 subunits. This creates a slow-moving form of Rdh54 that is the active form of the enzyme during HR. We further define mutants of Rdh54 that represent fast- and slow-moving forms of the enzyme. We find that these mutants have impacts on repair outcomes reflecting an interaction with the HR decision making tree. Finally, we hypothesize that reducing the translocation rate of Rdh54 through phosphorylation influences repair decisions during HR by regulation the transition between DNA sequence alignment and D-loop expansion.

Results

A Rdh54 phosphorylation mutant displays enhanced sensitivity to DNA damage

Rdh54 is a known target of the Mec1/Rad53 kinases (Ferrari *et al.*, 2013). However, the effects of Rdh54 phosphorylation during DNA repair are unknown. To identify potential phosphorylation sites, we used the SuperPhos database (Lanz *et al*, 2021). Nine phosphorylation sites were identified in Rdh54: S21, S53, S167, S387, S621, S790, S791, T851, and S852. Of these sites, one was part of a Rad53 consensus sequence (S852) (Sidorova & Breeden, 2003), and three were high confidence sites. High confidence sites are defined as >10 peptides identified in the proteomic analysis (S53, S621, and S852) (**Fig EV1A**). We initially converted all suspected phosphorylation sites to alanine and tested them for their ability to complement methyl-methanosulfonate (MMS) and camptothecin (CPT) sensitivity phenotypes in *rdh54*Δ haploid yeast strains. In addition to the serine/threonine to alanine mutations, we also tested the *rdh54K318R* allele which harbors a mutation in the Walker A box of Rdh54 preventing hydrolysis of ATP. We used this mutant because it has enhanced growth sensitivity phenotypes relative to the *rdh54*Δ strain. This was used as a comparison in case any of the phosphorylation mutants had similar phenotypes. Most of the S to A mutations complemented the weak MMS and CPT phenotypes associated with the *rdh54*Δ (**Fig EV1B**). However, one mutant, *rdh54T851A*, had enhanced sensitivity to CPT and MMS like *rdh54K318R* (**Fig EV1B**). Based on this result we also made the *rdh54K318R,T851A* double mutant. We found that the double mutant had similar defects to that of the single mutants, suggesting the mutations were affecting the same property of Rdh54.

We used the Alphafold2 predicted structure of Rdh54 to produce a molecular model of Rdh54 bound to a short fragment of dsDNA (**Fig 1A**). We aligned the Alphafold2 model of Rdh54 to an existing *Sulfolobus solfataricus* Snf2 DNA translocase structure bound to dsDNA (**PDBID:1Z63**) (Dürr *et al*, 2005). Because the *S. solfataricus* crystal structure represents the open form of the enzyme, we also created a closed model of Rdh54 by rotating one of the RecA domains (**Fig EV 2**) using the procedure from the original study (Dürr *et al.*, 2005). The closed form of the structure represents the active form of the enzyme (**Fig 1A and Fig EV2**). We were surprised to find that the T851 residue was located a large distance from the enzyme active site at the end of an alpha-helix predicted to extend along the dsDNA. The modelled structure of the alpha helix has a region of high confidence (90>pLDDT>70, cyan) at the C-terminal end, with less confidence predicted for the interior (70>pLDDT>50, yellow). Both T851 and S852 are in a disordered region at the C-terminus of the alpha helix. The SuperPhos database (Lanz *et al.*, 2021) found S852 to be phosphorylated more frequently than the T851 residue (57 peptides versus 3 peptides) *in vivo*, suggesting the S852 residue may be the primary target of phosphorylation *in vivo* and not the T851 residue. The MMS and CPT phenotypes associated with T851, its proximity to S852, and the high frequency of reported S852 phosphorylation, led us to hypothesize that these two residues could work in concert to regulate Rdh54 activity.

Mutation of phosphor-sites alters interhomolog recombination

Genetic experiments have implicated *RDH54* in regulating interhomolog (IH) gene conversion (Klein, 1997; Shinohara *et al.*, 1997). The mechanism behind this activity is an open question. We hypothesized that phosphorylation may contribute to interhomolog gene conversion. We tested *rdh54T851A*, *rdh54T851D, rdh54S852A*, *rdh54S852D,* and *rdh54T851A,S852A* alleles for their ability to promote interhomolog gene conversion. We used an assay that measures the spontaneous gene conversion of two inactive *leu2* alleles (*leu2-EcoR1* and *leu2-BstEII*) located on homologous chromosomes into an active *LEU2* gene (**Fig 1B**). The frequency of conversion events is measured by comparing growth on selective and non-selective media. WT strains had a *Leu+* frequency of $1.03+/-0.33x10^{-5}$ (**Fig 1C, Table 1**) that was not significantly different from the *rdh54*Δ strains, which had a conversion frequency of $0.92+/-0.5x10^{-5}$ (**Fig 1C, Table 1**). In contrast, the *rdh54T851A* and *rdh54S852A* strains had a significant reduction in *Leu+* frequencies of $0.3+/-0.19x10^{-5}$ and $0.44+/-0.21x10^{-5}$, respectively ($p<0.0001$and $p=0.0004$). The two phosphomimic versions of Rdh54, *rdh54T851D* and *rdh54S852D*, were comparable to WT in conversion frequencies ($0.9+/-0.15x10^{-5}$ and $0.88+/-0.19x10^{-5}$, respectively) (**Fig 1C, Table 1**). Surprisingly, the conversion frequency observed for the *rdh54T851A,S852A* double mutant was $1.03+/-0.44x10^{-5}$ and comparable to WT (**Fig 1C**). This suggests the *rdh54T851A,S852A* allele may be a compensatory mutation. From these data we conclude that *rdh54T851A* and *rdh54S852A*, and by extension the loss of phosphorylation, have a negative impact on IH gene conversion.

When using the homologous chromosome as a template for repair, LOH events can also occur by both reciprocal (CO) and non-reciprocal (BIR) exchange of DNA sequences between chromosomes. *RDH54* has previously been shown to reduce BIR outcomes, and to reduce CO frequency when the allele is inactivated by a mutation to the Walker A box, *rdh54K318R* (Keymakh *et al.*, 2022; Piazza *et al.*, 2019). For this reason, we hypothesized that our mutants may also affect CO or BIR outcomes. To test this hypothesis, we used a previously described genetic reporter assay that monitors LOH outcomes (Ho *et al*, 2010; Klein *et al*, 2019). The reporter is based on an *I-Sce1* site located in an inactive copy of the *ade2* gene on budding yeast chromosome

XV. The homologous chromosome has a different, but also inactive, allele of *ade2*. Upon *I-Sce1* induction with galactose both sister chromatids are cut, and repair occurs using the homologous chromosome as a template. Each homolog contains a different antibiotic marker located 154 kbp downstream of the break site (**Fig 2A**). Therefore, this assay can differentiate between long tract gene conversion (LTGC), short tract gene conversion (STGC), CO, NCO, and BIR outcomes associated with gene conversion events (Ho *et al.*, 2010; Klein *et al.*, 2019) (**Fig 2AC**).

The clearest determinant of repair outcomes can be seen when one sister is repaired by STGC, and the other by LTGC, resulting in sectored colonies. These colonies have undergone the first chromosomal division after plating and provide the easiest interpretation of the genetic outcomes following the DSB. For the purposes of this study, we are reporting only outcomes for red/white sectored colonies. When repair is forced to occur through the homologous chromosome, *rdh54*Δ and *rdh54K318R* strains do not show a significant drop in gene conversion (Keymakh *et al.*, 2022). This was also true for all the mutant alleles tested here (**Fig2B**), and there was no difference in the ratio of LTGC versus STGC (**Fig EV3**). Importantly, *rdh54T851A* and *rdh54S852A* alleles are not defective in gene conversion efficiencies following an induced DSB . Because they are defective in spontaneous gene conversion, we interpret this result to mean that these alleles cause defects in template selection.

Most of the alleles tested also had changes in the distribution of HR outcomes **(Fig 2DEF, Table 1**). A general reduction in CO outcomes was observed in *rdh54T851A* (10+/-1.7%, p<0.0001), *rdh54T851D* (36.7+/-8%, p=0.0069), *rdh54S852D* (16.9+/-3.4%, p<0.0001), and *rdh54S852A* (25.2+/-3.6%, p<0.0001) as compared to WT (53+/-10%) (**Fig 2D**). Surprisingly, the *rdh54T851A,S852A* allele was again compensatory and there was no significant difference in CO outcomes relative to the WT. There was also an increase in NCO outcomes associated with most of these alleles. In the case of the *rdh54T851A* allele (86.7 +/-0.5%) the magnitude of this change was proportional to the loss of CO outcomes (**Fig 2E, Table 1**). With *rdh54T851D* (53.7+/-8%, p=0.03), *rdh54S852A* (58.6+/-3.2%, p=0.0008), and *rdh54S852D* (16.9+/-3.4%, p<0.0001) these changes were also accompanied by an increase in BIR outcomes (**Fig 2F, Table 1**). The magnitude of the increase in BIR was greatest in the *rdh54S852A* strain (16.1+/-3.4%, p<0.0001), with smaller changes in *rdh54T851D* (9.4+/-1.8%, p=0.0026) and *rdh54S852D* (9.4+/-2.8%, p=0.01). The *rdh54T851A,S852A* was compensatory in all cases and indistinguishable from WT. From these data we conclude that the T851 and S852 residues in Rdh54 are regulatory sites during template selection and D-loop maturation.

We previously proposed that an increase in BIR observed in a *rdh54*Δ strain could result from an increase in DNA template switching during the BIR reaction. Accordingly, we tested whether the *rdh54S852A* allele would be defective in template switching. We used a previously characterized yeast strain (Anand *et al*, 2014) that was designed to test template switching outcomes during BIR by reconstitution of a *URA3* marker located at three distinct sites on chromosome III (Anand *et al.*, 2014) (**Fig EV4A**). DSBs were induced by overexpression of the HO nuclease leading to cleavage of a unique HO site. The frequency of *Ura*+ cells was measured for WT, *rdh54T851A*, *rdh54T851D*, *rdh54S852A*, *rdh54S852D*, and *rdh54T851A,S852A* strains. A *Ura*+ frequency of 16.5+/-0.4x10^{-5} was measured for WT strains and served as a reference for comparison with the Rdh54 mutants. There was a significant reduction in *Ura*+ frequency observed in the *rdh54T851A* (7.36+/-0.6x10^{-5} *Ura*+, p<0.0001) strain, and a partial reduction in the *rdh54S852D* (10.2+/-

$1.10x10^{-5}$ *Ura+*, p=0.001) and *rdh54T851A,S852A* ($11.6+/-2.3x10^{-5}$ *Ura+*, p=0.02) strains (**Figure EV4B, Table 1**). It should be noted that the *rdh54T851A,S852A* allele partially compensates for the *rdh54T851A* mutation as it does in other assays. Surprisingly, there was no significant difference observed in the *rdh54S852A* (p=0.12) or the *rdh54T851D* (p=0.17) strains. This suggests that the observed increase in BIR associated with *rdh54S852A* is not due to a reduction in template switching activity. In addition, we also conclude that the *rdh54T851A* allele shows a small reduction in template switching.

Biochemical analysis of Rdh54 mutants reveal a reduction in translocation

Several of the mutants we tested share phenotypes with the *rdh54K318R* allele (Keymakh *et al.*, 2022). There were also subtle differences in the phenotypes observed for each mutant. Based on this observation we hypothesized that these phenotypes may be caused by alterations in Rdh54 ATPase activity, and, by extension, movement along dsDNA. To test this, we overexpressed and purified 6xHis-Rdh54 and 6xHis-Rdh54T851A, 6xHis-Rdh54T851D, 6xHis-Rdh54S852A, 6xHis-Rdh54S852D, 6xHis-Rdh54T851AS852A, as well as mCherry versions of each protein from *E. coli* to measure ATP hydrolysis and single molecule translocation activity on dsDNA. The 6xHis tag on this protein does not have detrimental effects on protein activity (Crickard *et al.*, 2020a). Throughout this study we will use recombinant 6xHis-Rdh54. For simplicity we will omit using the 6xHis nomenclature in the remainder of the text.

First, we performed saturation enzyme kinetics on WT, Rdh54T851A, Rdh54S852A, Rdh54T851D, Rdh54S852D, and Rdh54T851AS852A proteins (**Fig 3A**). We compared Michaelis-Menten (MM) and Allosteric Sigmoidal (AS) models for fitting the ATP hydrolysis data. Surprisingly, we found that an AS model was a better fit for most of the data including the WT-Rdh54. We used the AS model to fit the ATPase data and calculated a V_{max} of 38.37 +/- 2.5 µM ADP/min, a $K_{0.5}$ of 245 +/-24 µM ATP, and an h-value (cooperativity factor, hill coefficient) of 2.2+/-0.4 (**Fig 3AB**) for WT-Rdh54. These data show that Rdh54 is cooperative and functions as at least a dimer during ATP hydrolysis. Rdh54T851D was comparable to WT in every metric (**Fig3AB**). In contrast, Rdh54T851A was different, with a V_{max} of 60 +/-4 µM ADP/min, a $K_{0.5}$ of 724 µM ATP, and an h-value of 1.6+/-0.2, indicating a defect in the ATPase activity.

Interestingly, an AS model did not fit the data as well for the Rdh54S852A, S852D, and T851AS852A mutants, which likely stems from significant changes in h-values (0.8 for Rdh54S852A and 5.6 for Rdh54S852D). To provide a direct comparison with WT, T851A, and T851D, we have reported fits of all data using an AS model (**Fig 3AB**). However, the fits for the Rdh54S852A, S852D, and T851AS852A data should be considered low confidence for a precise quantitative value. Qualitatively, Rdh54S852A and S852D have opposite effects on the cooperative behavior of Rdh54. This is consistent with phosphorylation being an important regulator of enzymatic activity. From these data we conclude that Rdh54 follows allosteric regulatory behavior, and that Rdh54T851A is defective in ATPase activity (**Fig 3AB**). We also conclude that the Rdh54S852A and Rdh54S852D mutants have opposite effects on Rdh54 enzymatic cooperativity.

We used DNA curtains, a fluorescent single molecule imaging approach, to measure the movement of Rdh54 along dsDNA (**Fig 3CD**). We measured the activity of WT-Rdh54 and its phosphomimic mutants using a Rdh54-mCherry fusion protein. Similar fluorescent constructs are active *in vivo*

(Lisby *et al.*, 2004). For WT Rdh54-mCherry, we measured a translocation velocity of 85+/-51 bp/sec (N=48), and a translocation distance of 12.1+/-7.1 kbp (N=48) (**Fig 3DEF**). Both observations are consistent with previous measurements made in different laboratories (Nimonkar *et al.*, 2007; Prasad *et al.*, 2007). For the Rdh54T851A mutant we observed a significant reduction in both mean velocity (35.4+/-26 bp/sec, N=81, p=<0.0001) and mean track length (5.1+/-3.0 kbp, N=81, p<0.0001). In contrast, the Rdh54T851D mutant was not significantly different from WT in either mean velocity (86+/-60 bp/sec, N=40, p=0.877) or mean track length (12.0+/-7.8 kbp, N=40, p=0.9), consistent with the results from the ATP hydrolysis experiments.

The Rdh54S852A mutant translocated with a mean velocity of 77 +/-54 bp/sec (N=41) and a mean translocation distance of 9.3+/-5.6 kbp (N=41). These values were not significantly different from the WT. In contrast, Rdh54S852D had a significant decrease in velocity (48.3+/-33.3 bp/sec, N=60, p<0.0001) and a small decrease in track length (9.3+/-6.5 kbp, N=60, p=0.03) relative to WT (**Fig 3DEF**). When combined with the ATP hydrolysis results, the S852A and S852D mutants have inverse behaviors relative to WT. These data suggest that phosphorylation makes Rdh54 more cooperative, which leads to a reduced translocation velocity. Finally, we tested the activity of the Rdh54T851AS852A mutant. We found this mutant had higher mean velocity (55+/-46 bp/sec) than the Rdh54T851A single mutant but was still significantly less than WT (p =0.0007, N=101). We saw an insignificant difference in track length (11.0+/-7.1 kbp, p=0.34) (**Fig 3DEF**) compared to the WT. This suggests that part of the observed compensatory mutation effect may stem from changes in biochemical activity and is likely related to a reduction in cooperativity between subunits during translocation in the double mutant. It further suggests that the native S852 residue regulates Rdh54 cooperativity in the absence of phosphorylation. From these data we conclude that both Rdh54T851 and Rdh54S852 have biochemical effects on Rdh54 enzymatic activity.

Rdh54 is a functional oligomer

Biochemically, Rdh54 forms a homo-oligomer in solution. Our data defines Rdh54 as a cooperative ATPase. To directly visualize this behavior, we tested the oligomeric activity of Rdh54 by mixing Rdh54-mCherry and Rdh54-GFP and monitoring translocation along dsDNA. Rdh54-mCherry colocalized with Rdh54-GFP in 93% of cases (**Fig 4A**, n=132/142) indicating an interaction between the two populations of molecules. The mixed molecules co-translocated with a mean velocity of 68.5+/-40.4 bp/sec, a mean distance of 14.3+/-8.8 kbp (**Fig 4BCD**) and were indistinguishable from un-mixed Rdh54-mCherry (N=32 and N=32, p=0.13 and p=0.22, respectively). When we mixed an equal molar amount of Rdh54-mCherry with Rdh54K318, the mean velocity was reduced to 30.7+/-20 bp/sec (N=62, p=<0.0001), representing a significant change from WT (**Fig 4CD**). Similarly reduced rates of translocation (23+/-16 bp/sec, N=31, p=<0.0001) (**Fig 4CD**) were observed when Rdh54T851A was mixed with equimolar amounts of WT. These data support an oligomeric motor configuration of Rdh54 in which translocation is contingent on the activity of adjacent protomers.

Next, we reasoned that if oligomer formation had an impact on HR outcomes, then strains that were heterozygous for *rdh54k318R* and *rdh54T851A* alleles would have altered CO/NCO ratios. We performed red/white recombination experiments with *RDH54:rdh54K318R* and *RDH54:rdh54T851A* strains. We found that the *RDH54:rdh54K318R* had a reduction in CO (27.3+/-4.0% versus 53 +/-10%, p=0.005) in favor of NCO (67.9+/-6% versus 41+/-10%, p=0.004)

outcomes. Likewise, there was a reduction in CO (34+/-9% versus 53+/-10%, p=0.002) and an increase in NCO outcomes (64.2+/-7% versus 41+/-10%, p=0.003) in the *RDH54:rdh54T851A* strain (**Fig 4E**). From these data we conclude that Rdh54 forms a biologically active oligomer during DNA damage response, and that its activity is likely modulated by inter-subunit communication.

Rad53 directly regulates the activity of Rdh54

The existing data suggest that Rad53 is responsible for phosphorylation of Rdh54 and of the Rdh54S852 site (Ferrari *et al.*, 2013). Based on our data, phosphorylation would create a more cooperative but slower form of Rdh54. Therefore, we tested whether an interaction could form between Rdh54 and Rad53. Rdh54-HA co-immunoprecipitates with Rad53 both with and without a DSB (**Fig 5AB and Fig EV5**) indicating a strong interaction between the two proteins. We next reconstituted this interaction *in vitro* using purified Rad53 and GFP-Rad53 from *E. coli*. These proteins retain auto kinase function and can be purified in the phosphorylated form (**Fig EV6A**). We measured binding of GFP-Rad53 to Rdh54-mCherry using single molecule imaging by visualizing GFP-Rad53 and Rdh54-mCherry co-bound to individual dsDNA molecules. We quantified the percentage of Rdh54-mCherry molecules that colocalized with GFP-Rad53 when bound to dsDNA (**Fig 5C**). At 10 nM GFP-Rad53, 31.5+/-0.9 % of Rdh54 molecules co-localized with GFP-Rad53, and at 100 nM, 65+/-22% of Rdh54 molecules co-localized with GFP-Rad53 (**Fig 5D**). It should be noted that GFP-Rad53 did not bind to dsDNA in the absence of Rdh54. In some instances, GFP-Rad53 was also observed to co-translocate with Rdh54-mCherry (**Fig EV6CD**). The interaction between Rad53 and Rdh54 resulted in phosphorylation as assayed using an *in vitro* kinase reaction with purified protein (**Figure EV6B**). From these data we conclude that Rad53 and Rdh54 form a strong interaction, and that Rad53 can directly phosphorylate Rdh54.

Finally, we tested the effects of direct Rdh54 phosphorylation by Rad53 using single molecule imaging. Our expectation based on data from the Rdh54S852D mutant was that phosphorylation of WT-Rdh54 would reduce the translocation velocity of WT-Rdh54. Likewise, phosphorylation would have no effect on the translocation velocity of the Rdh54S852A mutant. We incubated Rdh54-mCherry with Rad53 for 60 minutes prior to measuring the translocation velocity via single molecule imaging. Rdh54 treated with Rad53 moved with a translocation velocity of 42+/-21 bp/sec (**Fig 5E,** N=140). This was significantly (p<0.0001) different from the translocation velocity observed for untreated Rdh54, and comparable to the translocation velocity observed for Rdh54S852D. The track length for Rad53-treated Rdh54 (9.5+/-4.5 kbp) (**Fig 5F,** N=140) was only slightly lower than that observed for WT and was the same as Rdh54S852D. For Rad53-treated Rdh54S852A we observed no reduction in velocity relative to measurements from untreated Rdh54S852A (84.9+/-57 bp/sec, N= 66 versus 77+/-54 bp/sec, N=42, p=0.48) (**Fig 5E**); the same was also true for track length (**Fig 5F**). From these experiments we conclude that phosphorylation of Rdh54S852 by Rad53 results in a reduction in translocation velocity.

Discussion

Here we have defined the regulatory mechanism by which Rad53 controls Rdh54 during HR. Mutagenesis of phosphorylation sites in Rdh54 resulted in fast and slow translocating mutants of Rdh54. These mutants reveal a complex phenotype which illustrates that Rdh54 must be activated and deactivated during specific stages of HR. We hypothesize that Rdh54 uses motor function in

a supporting role to manage the lifetime of key HR reaction intermediates, and that coordination of this activity with damage signaling kinases is an important regulatory step.

Rdh54 is directly connected to Rad53

Rdh54 is a target of the Mec1/Rad53 signaling axis (Ferrari *et al.*, 2013), and physically interacts with the effector kinase Rad53. We identified one of the Rad53 phosphorylation sites by testing probable phosphorylation sites from the SuperPhos database. We found that mutations at the Rdh54T851 and Rdh54S852 residues caused several unique phenotypes. The Rdh54S852 site was part of a consensus Rad53 half-site (Lee *et al.*, 2003; Sidorova & Breeden, 2003), and is the biologically active kinase site. The consequence of phosphorylation at the S852 site is a reduction in Rdh54 motor function. Motor function was also compromised in several mutants in our study including Rdh54T851A and Rdh54S852D. These mutants had distinct defects in ATP hydrolysis. The Rdh54T851A mutant had an increased $K_{0.5}$, which could be due to changes in ATP binding or ATP hydrolysis. The Rdh54S852D had higher cooperativity leading to a decrease in the $K_{0.5}$. Like the phosphorylated version of the WT enzyme, this mutant was slower to translocate on the dsDNA. In contrast, Rdh54S852A was no longer cooperative. This resulted in more efficient translocation in single molecule experiments which was comparable to WT translocation. These data suggest that phosphorylation improves cooperativity of the enzyme, which leads to reduced motor function on dsDNA.

We hypothesize that changes in motor function are caused by alterations in Rdh54 inter-subunit communication. Rdh54 forms at least a homodimer in solution and is likely a homooligomer when bound to dsDNA (Prasad *et al.*, 2007) and is a functional oligomer on dsDNA. This translated to dosage dependent genetic effects on CO/NCO outcomes and is indicative of multimer function *in vivo*. Allosteric regulation of ATP hydrolysis could occur through interactions between adjacent subunits of Rdh54. The predicted structure of a Rdh54 monomer places the Rad53 kinase site far from the active site and provides a rational explanation for how phosphorylation may regulate inter-subunit communication. A similar mechanism for disruption of Rad51 binding to DNA has also been reported. Phosphorylation of Rad51 at the protomer interface prevents the formation of oligomers, and DNA binding (Flott *et al*, 2011). If the Rdh54 regulatory site is also on the protomer-protomer interface, then it is likely that phosphorylation of this site will prompt better communication between subunits creating a functional slow-moving Rdh54 oligomer. In this case the reason for modification is to stabilize HR intermediates. While this model cannot be directly tested without a high-resolution structure of a Rdh54, it is a feasible hypothesis.

Rdh54 translocation rate stabilizes HR intermediates

The activity of Rdh54 has been implicated in several different stages during HR. Examples include D-loop metabolism (Keymakh *et al.*, 2022; Piazza *et al.*, 2019), IH gene conversion (Klein, 1997; Shinohara *et al.*, 1997), alteration in HR outcome choice, chromosome mis-segregation (Sharp *et al.*, 2018), and checkpoint adaptation (Ferrari *et al.*, 2013). In each case null phenotypes are relatively minor and do not cause failure in HR. This led to the hypothesis that Rdh54 is an important feature in the selection of HR outcomes, but not completion of HR. We identified mutants in Rdh54 that we propose cause fast and slow motor function on dsDNA. These mutants are caused by a combination of mechanical defects in translocation (T851A, S852D), and loss of a phosphorylation site (S852A). Both slow and fast classes of Rdh54 mutants caused effects on the distribution of HR outcomes that are associated with template selection and second end capture.

Template selection occurs during the homology search stage of HR. Typically, the sister chromatid is rapidly selected and used as a template for repair. In mitotic cells, if the homology search persists for longer periods of time then the homolog can be selected (Bzymek *et al.*, 2010). In either case selection of the template requires a sequence alignment step followed by a D-loop expansion step (Fig. 6A). Disruption to the timing of either step can alter the probability of template choice and completion of repair. We observed that both fast and slow versions of Rdh54 have a 2-3-fold reduction in IH gene conversion outcomes. Rdh54 stabilizes both the presynaptic Rad51 filament (PSC) and early D-loop intermediates (Keymakh *et al.*, 2022; Meir *et al.*, 2022), and it is likely that these mutants are affecting the transition between sequence alignment and D-loop expansion.

The fast *rdh54S852A* mutant changes the frequency of IH gene conversion. It is possible that *rdh54S852A* is not properly recruited to sites of HR due to loss of phosphorylation. However, we think this scenario is unlikely because *rdh54T851A,S852A* has normal function. The second scenario is that *rdh54S852A* fails to form the cooperative slow-moving form of the enzyme, leading to rapid D-loop expansion and increased sister chromatid usage by decreasing the lifetime of the homology search. Surprisingly, the *rdh54*Δ strains were not defective in IH recombination. This can still be consistent with our model as PSCs that form in the absence of Rdh54 will be structurally distinct from those that form when Rdh54 is present and would be more susceptible to disassembly by Srs2 (Antony *et al*, 2009; Meir *et al.*, 2022). This could lead to decreased stability of PSCs and an increase in the lifetime of the homology search, compensating for the loss of Rdh54. The *rdh54S852D* allele was not defective in IH gene conversion and is consistent with phosphorylation promoting a slow form of Rdh54 that regulates the transition between sequence identification and D-loop expansion.

The slow *rdh54T851A* mutant was also defective in IH gene conversion. Our interpretation is that HR intermediates that are over stabilized may be more resistant to processing and delay completion of repair. This is essentially the opposite effect of the *rdh54S852A allele*. In this context we would expect the slow mutants of Rdh54 to be defective in general recombination and not just IH gene conversion. This is the case as *rdh54T851A* is sensitive to MMS treatment and has general defects in DNA repair. Furthermore, this is also consistent with previous reports that the *rdh54K318R* allele is defective in general gene conversion experiments and CO formation (Piazza *et al.*, 2019). In essence the Rdh54T851A mutant is acting as a persistent barrier that is not properly deactivated.

The comparison of *rdh54T851A* and *rdh54S852D* indicates that the motor output of defective mutants impacts the severity of phenotypes observed in both IH gene conversion and HR outcome experiments. The *rdh54T851A* mutant is more defective *in vitro* and can still be phosphorylated *in vivo*, leading to the more pronounced defect relative to *rdh54S852D*. The phenotypes are suppressed in the *rdh54T851A,S852A* mutant which moves slower and cannot be phosphorylated. This indicates the lack of phosphorylation can be overcome by sufficient reduction in motor function caused by the defect associated with the T851A mutant. In the natural setting it is likely that de-phosphorylation of Rdh54 will accompany proper processing of HR intermediates. Therefore, we propose that a cycle of phosphorylation and de-phosphorylation regulates Rdh54 activity at HR intermediates (**Fig 6A**). This regulates the transition between sequence alignment and D-loop expansion.

The second point of regulation affected by Rdh54 mutants is second end capture. We see that the fast mutant has a shift in HR outcomes that decrease CO outcomes in response to increases in BIR and NCO outcomes. This is consistent with a model where premature D-loop expansion of HR intermediates may prevent the proper capture of the second end of DNA required for the formation of CO products (**Fig 6B**). This argument is also supported by the slow mutant. The increase in NCO outcomes at the expense of CO could reflect limitations on the size of D-loop expansion that may reduce the formation of crossover products (Shah *et al.*, 2020). Alternatively, failure to expand the D-loop may drive the reaction in favor of SDSA outcomes that result in NCO repair (**Fig 6C**). In this model the phosphorylation/de-phosphorylation model is likely to play an important role in this decision.

Rdh54 is not required for completion of HR. However, Rdh54 regulates the processing of HR intermediates that bias reactions to specific outcomes. Guidance through these intermediates is controlled by the translocation speed and motor output of Rdh54 which is downregulated by the effector kinase Rad53 (**Fig 6ABC**). Our model would implicate Rdh54 as an indirect regulator of overall HR timing with its translocation rate being the property controlled by the kinase signaling pathway. It has recently been discovered that Rad54-B in the *C. elegans* germline plays a supporting role during meiotic HR (Yamaya *et al*, 2022). This study also finds that the largest impact in rad54-B animals is when the kinase CHK2 is active, revealing a connection with kinase signaling networks that has also been observed in *S. cerevisiae*. Again, these observations link the Rdh54/RAD54B family to DNA damage signaling networks, suggesting these motor proteins provide a functional link between recombination intermediates and kinase signaling networks. Still more work will need to be done to understand this mechanism on the cellular level. However, our findings of fast and slow versions of Rdh54, and their genetic consequences have made this possible.

Data Availability Statement

The data in this manuscript is available upon request.

Acknowledgements

We would like to acknowledge Hannah Klein, Jim Haber, and Lorraine Symington for yeast strains used in this study. We would also like to thank Dirk Remus for the kind gift of the Rad53 overexpression plasmid. We would also like to acknowledge Eric Alani and Marcus Smolka for critical reading of the manuscript. We would also like to thank members of the Cornell R3 group and the Crickard laboratory for helpful input during development of the project.

Author contributions

JH purified proteins, performed experiments, analyzed data, and helped with the writing of the manuscript. BF performed experiments, analyzed data, and helped with writing and editing of the manuscript. JD provided reagents and cloning support. JBC performed experiments, analyzed data, provided reagents, and wrote the manuscript with input from JH and BF. This work was supported by NIGMS R35142457 to JBC and Cornell Startup funds to JBC.

Materials and Methods:

Yeast strain construction

Most of the *S. cerevisiae* strains used in this study were W303. All recombination outcome experiments were performed in the W303 background. Strains for spot assay experiments were BY4741 and were generated by transformation of *rdh54*Δ strains with pRS415 plasmids. The genotypes for all strains used in this study can be found in Extended Data Table 1.

Yeast spot growth assay

For complementation spot assays, overnight cultures were diluted back to an OD_{600} of 0.2 and then allowed to grow to an OD_{600} of 1.0. Cells were then serially diluted and manually spotted on Synthetic Complete (SC) -Leu plates containing either no drug, 0.01% MMS or 25 µM CPT. Plates were incubated at 30˚C for 2-3 days and imaged at 24, 48, and 72 hours.

Interhomolog gene conversion assay

Yeast strains of JBC206 and JBC207 and derivatives were crossed (Extended Data Table 1), and the diploids were selected on YNB (-Ura/-Trp) + 2% dextrose and allowed to grow for 2-3 days. Fresh diploid colonies were then grown for 15 hours in YPD. 30 µl of saturated culture was plated on YNB (-Leu) + 2% dextrose and 30 µl of culture diluted 1:10,000 was plated on YNB (SC) + 2% dextrose and allowed to grow for three days. The colonies on each plate were then counted. The data was analyzed by dividing the adjusted number of colonies on the -Leu plate by the colonies on the SC plate. This generated a frequency. The mean and standard deviation of the data was determined using multiple different colonies from multiple different crosses.

Red/White recombination assay

The WT strain used in this assay as well as the procedure for diploid formation are described here (Ho *et al.*, 2010; Keymakh *et al.*, 2022). The genotypes for modifications to these strains can be found in Extended Data Table 1. The assay was performed by growing the appropriate strain overnight in YP +2% raffinose. The next day cells were diluted to an OD_{600} of 0.2 and allowed to reach an OD_{600} of 0.4-0.5 followed by the expression of *I-Sce1* by the addition of 2% galactose. Cells were allowed to grow for an additional 1.5 hours, after which they were plated on YPD and allowed to grow for 48 hours. After 48 hours they were placed at 4˚C overnight to allow further development of red color. The number of white, red, and sectored colonies was then counted followed by replica plating onto YPD + hygromycin B (200 µg/ml) and YPD + nourseothricin (67 µg/ml, clonNat) for analysis of recombination outcomes. Technical duplicate plates were also plated onto YNB (+ade) +2% raffinose +2% galactose to measure reinduction of *I-Sce1*, indicating the fraction of cleaved sister chromatids. Finally, strains were also replica plated on YNB (-Ura/-Met) + 2% dextrose to insure proper chromosome segregation. The data was analyzed by counting colonies that were sectored, and then counting colony survival on different antibiotic sensitivities. The data for each category was then divided by the total population of sectored colonies. The

standard deviation between biological replicates analyzed for at least four independent experiments from different crosses.

Template switching assay

The WT strains used for this study were described in (Anand *et al.*, 2014). The genotypes for modification of these strains can be found in Extended Data table 1. The assay was performed by growing the appropriate strain in YP + 2% raffinose overnight. The next day cells were diluted in YP + 2% raffinose to an OD_{600} of 0.2 and allowed to grow for four hours. The cells were then treated with 2% galactose for 3 hours and plated on YNB (-Ura) + 2% dextrose. Colony forming units (CFU) were determined by plating a serial dilutions of the culture on non-selective media. After three days the plates were scored for colony growth. The *Ura+* frequency was determined by dividing the adjusted CFU from the selective plate by the number of colonies on the non-selective plate. The mean and standard deviation were calculated for three independent experiments.

Co-immunoprecipitation experiments

A starter culture was grown in 5 mL YPD for 10 hours. The culture was then inoculated into 100 mL of YP + 3% glycerol + 2% sodium lactate and allowed to grow overnight until the OD_{600} was ~1.0. Then 2% galactose (final concentration) was added to the culture to induce DSBs. In an uninduced control group, 2% dextrose was added. The cells were allowed to grow for 2 hours and harvested by centrifugation. Cell pellets were washed twice with 1xPBS (137 mM NaCl, 2.7 mM NaCl, 1.8 mM KH_2PO_4, 10 mM Na_2HPO_4) + 0.2 mM PMSF, and frozen at -80 ˚C for at least 30 minutes. Cells were then thawed and resuspended in lysis buffer (20 mM Tris-Cl pH 7.5, 300 mM KCl, 0.01% NP-40, 10% glycerol,0.2 mM PMSF, Protease inhibitor cocktail). Glass disruptor beads were added, and the cells were bead beat by a vortex with 1 minute on and 1 minute off for a total of 8 cycles. The cellular debris was then spun down at ~1,100 x g for 10 minutes at 4 ˚C. The supernatant was then centrifuged at 26,712 x g for 10 minutes at 4 ˚C. The supernatant was collected as whole cell extract and preincubated with anti-HA (Roche, 11583816001) for 1 hour at 4 ˚C and then incubated with Dynabeads Goat anti-mouse IgG (Invitrogen, Cat No. 11033) overnight at 4 ˚C. For each 1 mL of cell lysates, 1 µL of anti-HA antibody and 15 µL of Dynabeads were used. The immunocomplex were washed with wash buffer (20 mM Tris-Cl pH 7.5, 500 mM KCl, 0.01% NP-40, 10% glycerol) 3 times and transferred to a new tube. The whole cell extract and immunocomplex were dissolved in SDS loading buffer, subjected to SDS-PAGE, and transferred onto nitrocellulose membrane. The membrane was stained with Ponceau S staining solution (5% glacial acetic, 0.1% Ponceau S) and blocked with 5% non-fat dry milk in TBST (2.4 g Tris, 8.7 g NaCl, 1 mL Tween-20 in 1 L H_2O, pH 7.5) for 1 hour. The membrane was then incubated with the primary antibody (anti-Rad53, Abcam, ab104232, 1.3:1000) in 5% non-fat dry milk in TBST overnight at 4 ˚C followed by secondary antibodies (Goat anti-Mouse IgG, Invitrogen, Cat No. A16072, 1:3000) at room temperature for 1 hour. The immunoblots were visualized with enhanced chemiluminescence.

Protein expression and purification

6xHis-Rdh54, 6xHis-Rdh54-mCherry, and Rdh54 mutants were purified as follows. Rosetta 2 Bl21 (DE3) cells bearing pET15-6xHis-Rdh54 expression plasmids were grown to an OD_{600} between 0.6 and 0.8 at 37 ˚C. The temperature was lowered to 16 ˚C and cells were induced with

0.5 mM IPTG overnight. Cells were harvested by centrifugation and stored at -80˚C. Cells were resuspended in buffer A (25 mM Tris-HCl pH 7.5, 1000 mM NaCl, 10 mM Imidazole, 0.01% NP-40, 10% Glycerol, 5 mM 2-Mercaptoethanol, 0.2 mM PMSF, and Protease Inhibitor cocktail) and lysed by freeze thaw. Cell lysate was sonicated on ice with 10 cycles with 65% duty cycle and 15 sec on and 45 sec off. Lysate was centrifuged at 10,000 x g for 45 minutes at 4 ˚C. Clarified extract was mixed with pre-equilibrated His-Pur Nickel-NTA resin and incubated in batch for 1 hour at 4 ˚C. After 1 hour the resin was centrifuged and washed 2x with buffer A, followed by 2x washes with buffer B (25 mM Tris-HCl pH 7.5, 200 mM NaCl, 10 mM Imidazole, 0.01% NP-40, 10% Glycerol, 5 mM 2-Mercaptoethanol, 0.2 mM PMSF, and Protease Inhibitor cocktail). The resin was then added to a disposable column. The protein was eluted in buffer C (25 mM Tris-HCl pH 7.5, 200 mM NaCl, 200 mM Imidazole, 0.01% NP-40, 10% Glycerol, 5 mM 2-Mercaptoethanol, 0.2 mM PMSF, and Protease Inhibitor cocktail). Fractions were analyzed by SDS-PAGE and the peak fractions were pooled. The protein was further purified using a strong cation exchange column (HiScreen SP FF). The column was resolved using a 20-100% gradient of buffer D (25 mM Tris-Cl pH 7.5, 0 mM KCl, 1 mM EDTA, 0.01% NP-40, 5 mM 2-Mercaptoethanol, 10% Glycerol) and buffer E (25 mM Tris-Cl pH 7.5, 1000 mM KCl, 1 mM EDTA, 0.01% NP-40, 5 mM 2-Mercaptoethanol, 10% Glycerol). Fractions were analyzed by SDS-PAGE. Peak fractions were pooled and concentrated by centrifugation at ~1,100 x g at 4 ˚C using a 10 kDa MWCO Vivaspin 6 column. Protein was finally purified on a 120 mL S300 column (HiPrep Sephacryl S-300 HR) in SEC buffer (30 mM Na-Hepes pH 7.5, 400 mM NaCl, 1 mM EDTA, 0.01% NP-40, 5 mM 2-Mercaptoethanol, 10% Glycerol). Peak fractions were pooled, and the protein was concentrated as described above. Purified protein was stored at -80 ˚C. 6xHis-Rad53, 6xHis-GFP-Rad53 were purified as previously described (Devbhandari & Remus, 2020).

In vitro kinase reactions

In vitro kinase assays were performed in Rad53 kinase buffer (25 mM Na-Hepes pH 7.5,150 mM NaOAc, 10% Glycerol, 10 mM $MgCl_2$, 10 mM ATP, 0.2 mM Na Orthovanadate). 1 µM Rdh54 was incubated with 0.1 µM Rad53 for the defined periods of time. Reactions were quenched with SDS-PAGE loading buffer and resolved on a 10% SDS-PAGE impregnated with phostag reagent and 10 mM $MnCl_2$. The gel was stained with Coomassie Brilliant blue and the shift in Rdh54 was directly observed.

ATPase assay

To measure ATP hydrolysis rates, a commercially available ADP-GLO kit was used. ATP hydrolysis reaction were performed in HR buffer (20 mM Tris-OAc, 50 mM NaCl, 10 mM $MgOAc_2$, 200 ng/µl BSA, 1 mM DTT and 10% Glycerol) and contained 250 ng/µl sheared salmon sperm DNA, and 250 nM Rdh54. ATP was titrated and standard hydrolysis plots were generated from this data. The data was fit using GraphPad prism 9. To determine the appropriate model, model comparison was performed between Michaelis-Menten and Allosteric Sigmoid. The Allosteric Sigmoid model was most appropriate for WT RDH54 compared to a standard Michaelis-Menten curve, and the $K_{0.5}$, $V_{max,}$ and h-value were determined from this Allosteric Sigmoid fit. The experiments were conducted at least four times with multiple preps of enzyme.

Flow cell construction

To generate flow cells, metallic chrome patterns were deposited on quartz microscope slides with pre-drilled holes for microfluidic line attachment by electron beam lithography (Collins *et al*,

2014). After metal deposition microscope slides were converted to flow cells by adhering a piece of double-sided tape to the side of the microscope slide with the metal barriers. A channel was created by covering the two-sided tape with a small piece of paper in between the two drill holes. The paper was excised to create the flow chamber and a glass coverslip was fixed to the tape. The chamber was sealed by heating to 165˚C in a vacuum oven at 25 mm Hg for 60 minutes. Flow cells were then completed by using hot glue to fit IDEX nanoports over the drill holes on the opposite side of the microscope slide from the coverslip.

Single molecule experiments

All single molecule experiments were conducted on a custom-built prism-based total internal reflection microscope (Nikon) equipped with a 488-nm laser (Coherent Sapphire, 100 mW), a 561-nm laser (Coherent Sapphire, 200 mW), and two Andor iXon EMCCD cameras. DNA substrates for DNA curtains experiments were made by attaching a biotinylated oligo to one end of the 50 kb Lambda phage genome, and an oligo with a digoxygenin moiety on the other. This allowed double tethering of the DNA between chrome barriers and chrome pedestals, as previously described (Collins *et al.*, 2014; Crickard, 2023). Flow cells were attached to a microfluidic system and sample delivery was controlled using a syringe pump (KD Scientific). Two color imaging was achieved by two XION 512x512 back-thinned Andor EM-CCD cameras and alternative illumination using a 488-nm laser and a 561 nM laser at 25% power output. The lasers were shuttered resulting in a 200 msec delay between each frame. Images were collected with a 200 msec integration time. Rdh54-mCherry translocation velocity and distances were measured in HR Buffer (20 mM Tris-OAc, 50 mM NaCl, 10 mM $MgOAc_2$, 200 ng/µl BSA, 1 mM DTT).

Analysis of dsDNA translocation

The velocity and translocation distance for Rdh54-mCherry molecules were measured by importing raw TIFF images as image stacks into ImageJ. Kymographs were generated by defining a 1-pixel wide region of interest (ROI) along the long axis of individual dsDNA molecules. Data analysis was performed from the kymographs. The start of translocation was defined when the Rdh54-mCherry molecule moved > 2 pixels. Pauses were defined as momentary stalls in translocation that lasted 2-4 frames. Termination was defined by molecules that did not move for >10 frames. Velocities represent pause free velocities. Velocities were calculated using the following formula $[(|Y_f-Y_i|)*1{,}000\ bp/[|X_f-X_i|])*frame\ rate]$; where Y_i and Y_f correspond to the initial and final pixel position and X_i and X_f correspond to the start and stop time (in seconds). Graphs of individual velocity and distances travelled were plotted in GraphPad Prism 9. The mean was determined from these graphs and significant differences between mutants was determined by performing a student's t-test of this data.

Rad53 binding experiments

For Rdh54 binding experiments, 1 nM of 6xHis-Rdh54-mCherry was mixed with 6xHis-GFP-Rad53 (10 nM or 100 nM) and injected onto pre-formed DNA curtains. Initial binding was monitored with a frame rate of 1 frame/3 sec. Data were then processed as described above. The number of Rdh54 molecule bound by GFP-Rad53 were then scored for binding.

Bibliography

Agarwal R, Tang Z, Yu H, Cohen-Fix O (2003) Two Distinct Pathways for Inhibiting Pds1 Ubiquitination in Response to DNA Damage*. *Journal of Biological Chemistry* 278: 45027-45033

Alcasabas AA, Osborn AJ, Bachant J, Hu F, Werler PJH, Bousset K, Furuya K, Diffley JFX, Carr AM, Elledge SJ (2001) Mrc1 transduces signals of DNA replication stress to activate Rad53. *Nature Cell Biology* 3: 958-965

Anand RP, Tsaponina O, Greenwell PW, Lee C-S, Du W, Petes TD, Haber JE (2014) Chromosome rearrangements via template switching between diverged repeated sequences. *Genes & Development* 28: 2394-2406

Antony E, Tomko EJ, Xiao Q, Krejci L, Lohman TM, Ellenberger T (2009) Srs2 Disassembles Rad51 Filaments by a Protein-Protein Interaction Triggering ATP Turnover and Dissociation of Rad51 from DNA. *Molecular Cell* 35: 105-115

Bacal J, Moriel-Carretero M, Pardo B, Barthe A, Sharma S, Chabes A, Lengronne A, Pasero P (2018) Mrc1 and Rad9 cooperate to regulate initiation and elongation of DNA replication in response to DNA damage. *The EMBO Journal* 37: e99319

Bell JC, Kowalczykowski SC (2016) RecA: Regulation and Mechanism of a Molecular Search Engine. *Trends Biochem Sci* 41: 491-507

Bzymek M, Thayer NH, Oh SD, Kleckner N, Hunter N (2010) Double Holliday junctions are intermediates of DNA break repair. *Nature* 464: 937-941

Chen J-M, Cooper DN, Chuzhanova N, Férec C, Patrinos GP (2007) Gene conversion: mechanisms, evolution and human disease. *Nature Reviews Genetics* 8: 762-775

Chen S-h, Zhou H (2009) Reconstitution of Rad53 Activation by Mec1 through Adaptor Protein Mrc1*. *Journal of Biological Chemistry* 284: 18593-18604

Chi P, Kwon Y, Seong C, Epshtein A, Lam I, Sung P, Klein HL (2006) Yeast recombination factor Rdh54 functionally interacts with the Rad51 recombinase and catalyzes Rad51 removal from DNA. *J Biol Chem* 281: 26268-26279

Collins BE, Ye LF, Duzdevich D, Greene EC (2014) Chapter 12 - DNA curtains: Novel tools for imaging protein–nucleic acid interactions at the single-molecule level. In: *Methods in Cell Biology*, Waters J.C., Wittman T. (eds.) pp. 217-234. Academic Press:

Coutelier H, Xu Z, Morisse MC, Lhuillier-Akakpo M, Pelet S, Charvin G, Dubrana K, Teixeira MT (2018) Adaptation to DNA damage checkpoint in senescent telomerase-negative cells promotes genome instability. *Genes & Development* 32: 1499-1513

Crickard JB (2023) Single Molecule Imaging of DNA-Protein Interactions Using DNA Curtains. *Methods Mol Biol* 2599: 127-139

Crickard JB, Kwon Y, Sung P, Greene EC (2020a) Rad54 and Rdh54 occupy spatially and functionally distinct sites within the Rad51-ssDNA presynaptic complex. *The EMBO Journal* 39: e105705

Crickard JB, Moevus CJ, Kwon Y, Sung P, Greene EC (2020b) Rad54 Drives ATP Hydrolysis-Dependent DNA Sequence Alignment during Homologous Recombination. *Cell* 181: 1380-1394.e1318

Devbhandari S, Remus D (2020) Rad53 limits CMG helicase uncoupling from DNA synthesis at replication forks. *Nat Struct Mol Biol* 27: 461-471

Dürr H, Körner C, Müller M, Hickmann V, Hopfner KP (2005) X-ray structures of the Sulfolobus solfataricus SWI2/SNF2 ATPase core and its complex with DNA. *Cell* 121: 363-373
Ferrari M, Nachimuthu BT, Donnianni RA, Klein H, Pellicioli A (2013) Tid1/Rdh54 translocase is phosphorylated through a Mec1- and Rad53-dependent manner in the presence of DSB lesions in budding yeast. *DNA Repair (Amst)* 12: 347-355
Filippo JS, Sung P, Klein H (2008) Mechanism of Eukaryotic Homologous Recombination. *Annual Review of Biochemistry* 77: 229-257
Flott S, Kwon Y, Pigli YZ, Rice PA, Sung P, Jackson SP (2011) Regulation of Rad51 function by phosphorylation. *EMBO reports* 12: 833-839
Greene EC (2016) DNA Sequence Alignment during Homologous Recombination. *Journal of Biological Chemistry* 291: 11572-11580
Haber JE (2018) DNA Repair: The Search for Homology. *BioEssays* 40: 1700229
Ho CK, Mazón G, Lam AF, Symington LS (2010) Mus81 and Yen1 promote reciprocal exchange during mitotic recombination to maintain genome integrity in budding yeast. *Mol Cell* 40: 988-1000
Hügel A, Wernert N (1999) Loss of heterozygosity (LOH), malignancy grade and clonality in microdissected prostate cancer. *British Journal of Cancer* 79: 551-557
Hunter N (2015) Meiotic Recombination: The Essence of Heredity. *Cold Spring Harb Perspect Biol* 7
Kadyk LC, Hartwell LH (1992) Sister chromatids are preferred over homologs as substrates for recombinational repair in Saccharomyces cerevisiae. *Genetics* 132: 387-402
Keymakh M, Dau J, Hu J, Ferlez B, Lisby M, Crickard JB (2022) Rdh54 stabilizes Rad51 at displacement loop intermediates to regulate genetic exchange between chromosomes. *PLoS Genet* 18: e1010412
Klein HL (1997) RDH54, a RAD54 homologue in Saccharomyces cerevisiae, is required for mitotic diploid-specific recombination and repair and for meiosis. *Genetics* 147: 1533-1543
Klein HL, Bačinskaja G, Che J, Cheblal A, Elango R, Epshtein A, Fitzgerald DM, Gómez-González B, Khan SR, Kumar S *et al* (2019) Guidelines for DNA recombination and repair studies: Cellular assays of DNA repair pathways. *Microb Cell* 6: 1-64
Kockler ZW, Osia B, Lee R, Musmaker K, Malkova A (2021) Repair of DNA Breaks by Break-Induced Replication. *Annual Review of Biochemistry* 90: 165-191
Kowalczykowski SC (2015) An Overview of the Molecular Mechanisms of Recombinational DNA Repair. *Cold Spring Harb Perspect Biol* 7
Kramara J, Osia B, Malkova A (2018) Break-Induced Replication: The Where, The Why, and The How. *Trends Genet* 34: 518-531
Krishnan V, Nirantar S, Crasta K, Cheng AY, Surana U (2004) DNA replication checkpoint prevents precocious chromosome segregation by regulating spindle behavior. *Mol Cell* 16: 687-700
Kumar S, Buon L, Talluri S, Roncador M, Liao C, Zhao J, Shi J, Chakraborty C, Gonzalez G, Tai Y-T *et al* (2021) Integrated genomics and comprehensive validation reveal drivers of genomic evolution in esophageal adenocarcinoma. *Communications Biology* 4: 617
Lanz MC, Yugandhar K, Gupta S, Sanford EJ, Faça VM, Vega S, Joiner AMN, Fromme JC, Yu H, Smolka MB (2021) In-depth and 3-dimensional exploration of the budding yeast phosphoproteome. *EMBO Rep* 22: e51121

Lee PS, Petes TD (2010) From the Cover: mitotic gene conversion events induced in G1-synchronized yeast cells by gamma rays are similar to spontaneous conversion events. *Proc Natl Acad Sci U S A* 107: 7383-7388
Lee SE, Pellicioli A, Malkova A, Foiani M, Haber JE (2001) The Saccharomyces recombination protein Tid1p is required for adaptation from G2/M arrest induced by a double-strand break. *Current Biology* 11: 1053-1057
Lee SJ, Schwartz MF, Duong JK, Stern DF (2003) Rad53 phosphorylation site clusters are important for Rad53 regulation and signaling. *Mol Cell Biol* 23: 6300-6314
Lisby M, Barlow JH, Burgess RC, Rothstein R (2004) Choreography of the DNA damage response: spatiotemporal relationships among checkpoint and repair proteins. *Cell* 118: 699-713
Lisby M, Rothstein R (2015) Cell Biology of Mitotic Recombination. *Cold Spring Harbor Perspectives in Biology* 7
Malkova A, Ira G (2013) Break-induced replication: functions and molecular mechanism. *Current opinion in genetics & development* 23: 271-279
Mazin AV, Bornarth CJ, Solinger JA, Heyer WD, Kowalczykowski SC (2000) Rad54 protein is targeted to pairing loci by the Rad51 nucleoprotein filament. *Mol Cell* 6: 583-592
Mazloum N, Holloman WK (2009) Second-End Capture in DNA Double-Strand Break Repair Promoted by Brh2 Protein of Ustilago maydis. *Molecular Cell* 33: 160-170
McIlwraith MJ, West SC (2008) DNA Repair Synthesis Facilitates RAD52-Mediated Second-End Capture during DSB Repair. *Molecular Cell* 29: 510-516
Mehta A, Beach A, Haber JE (2017) Homology Requirements and Competition between Gene Conversion and Break-Induced Replication during Double-Strand Break Repair. *Molecular Cell* 65: 515-526.e513
Mehta A, Haber JE (2014) Sources of DNA Double-Strand Breaks and Models of Recombinational DNA Repair. *Cold Spring Harbor Perspectives in Biology* 6
Meir A, Crickard JB, Kwon Y, Sung P, Greene EC (2022) Rad54 and Rdh54 prevent Srs2-mediated disruption of Rad51 presynaptic filaments. *Proc Natl Acad Sci U S A* 119
Mordes DA, Nam EA, Cortez D (2008) Dpb11 activates the Mec1–Ddc2 complex. *Proceedings of the National Academy of Sciences* 105: 18730-18734
Moynahan ME, Jasin M (1997) Loss of heterozygosity induced by a chromosomal double-strand break. *Proceedings of the National Academy of Sciences* 94: 8988-8993
Navadgi-Patil VM, Burgers PM (2011) Cell-cycle-specific activators of the Mec1/ATR checkpoint kinase. *Biochem Soc Trans* 39: 600-605
Nichols CA, Gibson WJ, Brown MS, Kosmicki JA, Busanovich JP, Wei H, Urbanski LM, Curimjee N, Berger AC, Gao GF *et al* (2020) Loss of heterozygosity of essential genes represents a widespread class of potential cancer vulnerabilities. *Nature Communications* 11: 2517
Nimonkar AV, Amitani I, Baskin RJ, Kowalczykowski SC (2007) Single molecule imaging of Tid1/Rdh54, a Rad54 homolog that translocates on duplex DNA and can disrupt joint molecules. *J Biol Chem* 282: 30776-30784
Nimonkar AV, Sica RA, Kowalczykowski SC (2009) Rad52 promotes second-end DNA capture in double-stranded break repair to form complement-stabilized joint molecules. *Proceedings of the National Academy of Sciences of the United States of America* 106: 3077-3082
Palou R, Palou G, Quintana DG (2017) A role for the spindle assembly checkpoint in the DNA damage response. *Current Genetics* 63: 275-280

Petukhova G, Sung P, Klein H (2000) Promotion of Rad51-dependent D-loop formation by yeast recombination factor Rdh54/Tid1. *Genes Dev* 14: 2206-2215
Pham N, Yan Z, Yu Y, Faria Afreen M, Malkova A, Haber JE, Ira G (2021) Mechanisms restraining break-induced replication at two-ended DNA double-strand breaks. *The EMBO Journal* 40: e104847
Piazza A, Bordelet H, Dumont A, Thierry A, Savocco J, Girard F, Koszul R (2021) Cohesin regulates homology search during recombinational DNA repair. *Nature Cell Biology* 23: 1176-1186
Piazza A, Heyer WD (2019) Moving forward one step back at a time: reversibility during homologous recombination. *Curr Genet* 65: 1333-1340
Piazza A, Shah SS, Wright WD, Gore SK, Koszul R, Heyer WD (2019) Dynamic Processing of Displacement Loops during Recombinational DNA Repair. *Mol Cell* 73: 1255-1266.e1254
Prasad TK, Robertson RB, Visnapuu ML, Chi P, Sung P, Greene EC (2007) A DNA-translocating Snf2 molecular motor: Saccharomyces cerevisiae Rdh54 displays processive translocation and extrudes DNA loops. *J Mol Biol* 369: 940-953
Qi Z, Redding S, Lee JY, Gibb B, Kwon Y, Niu H, Gaines WA, Sung P, Greene EC (2015) DNA sequence alignment by microhomology sampling during homologous recombination. *Cell* 160: 856-869
Renkawitz J, Lademann CA, Jentsch S (2014) Mechanisms and principles of homology search during recombination. *Nat Rev Mol Cell Biol* 15: 369-383
Renkawitz J, Lademann CA, Kalocsay M, Jentsch S (2013) Monitoring homology search during DNA double-strand break repair in vivo. *Mol Cell* 50: 261-272
Roy U, Kwon Y, Marie L, Symington L, Sung P, Lisby M, Greene EC (2021) The Rad51 paralog complex Rad55-Rad57 acts as a molecular chaperone during homologous recombination. *Molecular Cell* 81: 1043-1057.e1048
Ryland GL, Doyle MA, Goode D, Boyle SE, Choong DYH, Rowley SM, Li J, Australian Ovarian Cancer Study G, Bowtell DDL, Tothill RW *et al* (2015) Loss of heterozygosity: what is it good for? *BMC Med Genomics* 8: 45-45
Sanford EJ, Comstock WJ, Faça VM, Vega SC, Gnügge R, Symington LS, Smolka MB (2021) Phosphoproteomics reveals a distinctive Mec1/ATR signaling response upon DNA end hyper-resection. *Embo j* 40: e104566
Schwartz MF, Lee SJ, Duong JK, Eminaga S, Stern DF (2003) FHA domain-mediated DNA checkpoint regulation of Rad53. *Cell Cycle* 2: 384-396
Scully R, Panday A, Elango R, Willis NA (2019) DNA double-strand break repair-pathway choice in somatic mammalian cells. *Nat Rev Mol Cell Biol* 20: 698-714
Shah PP, Zheng X, Epshtein A, Carey JN, Bishop DK, Klein HL (2010) Swi2/Snf2-Related Translocases Prevent Accumulation of Toxic Rad51 Complexes during Mitotic Growth. *Molecular Cell* 39: 862-872
Shah SS, Hartono S, Piazza A, Som V, Wright W, Chédin F, Heyer WD (2020) Rdh54/Tid1 inhibits Rad51-Rad54-mediated D-loop formation and limits D-loop length. *Elife* 9
Sharp NP, Sandell L, James CG, Otto SP (2018) The genome-wide rate and spectrum of spontaneous mutations differ between haploid and diploid yeast. *Proceedings of the National Academy of Sciences* 115: E5046-E5055

Shinohara M, Shita-Yamaguchi E, Buerstedde JM, Shinagawa H, Ogawa H, Shinohara A (1997) Characterization of the roles of the Saccharomyces cerevisiae RAD54 gene and a homologue of RAD54, RDH54/TID1, in mitosis and meiosis. *Genetics* 147: 1545-1556
Sidorova JM, Breeden LL (2003) Rad53 checkpoint kinase phosphorylation site preference identified in the Swi6 protein of Saccharomyces cerevisiae. *Mol Cell Biol* 23: 3405-3416
Sugawara N, Wang X, Haber JE (2003) In vivo roles of Rad52, Rad54, and Rad55 proteins in Rad51-mediated recombination. *Mol Cell* 12: 209-219
Swift LH, Golsteyn RM (2016) Chapter 22 - The Relationship Between Checkpoint Adaptation and Mitotic Catastrophe in Genomic Changes in Cancer Cells. In: *Genome Stability*, Kovalchuk I., Kovalchuk O. (eds.) pp. 373-389. Academic Press: Boston
Symington LS, Rothstein R, Lisby M (2014) Mechanisms and regulation of mitotic recombination in Saccharomyces cerevisiae. *Genetics* 198: 795-835
Szostak JW, Orr-Weaver TL, Rothstein RJ, Stahl FW (1983) The double-strand-break repair model for recombination. *Cell* 33: 25-35
Tavares EM, Wright WD, Heyer W-D, Le Cam E, Dupaigne P (2019) In vitro role of Rad54 in Rad51-ssDNA filament-dependent homology search and synaptic complexes formation. *Nature Communications* 10: 4058
Waterman DP, Haber JE, Smolka MB (2020) Checkpoint Responses to DNA Double-Strand Breaks. *Annu Rev Biochem* 89: 103-133
Wu X, Malkova A (2021) Break-induced replication mechanisms in yeast and mammals. *Current Opinion in Genetics & Development* 71: 163-170
Wyman C, Kanaar R (2006) DNA Double-Strand Break Repair: All's Well that Ends Well. *Annual Review of Genetics* 40: 363-383
Xu J, Zhao L, Xu Y, Zhao W, Sung P, Wang HW (2017) Cryo-EM structures of human RAD51 recombinase filaments during catalysis of DNA-strand exchange. *Nat Struct Mol Biol* 24: 40-46
Yamaya K, Wang B, Memar N, Odiba AS, Woglar A, Gartner A, Villeneuve AM (2022) Disparate roles for *C. elegans* DNA translocase paralogs RAD-54.L and RAD-54.B in meiotic prophase germ cells. *bioRxiv*: 2022.2012.2012.520157

Figure 1

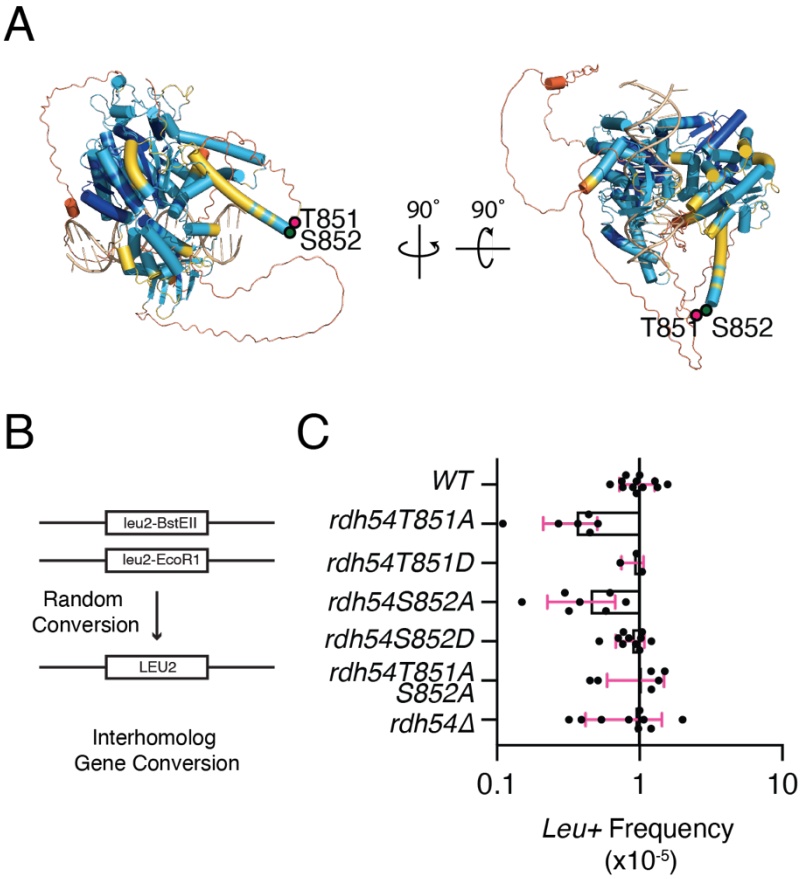

Figure 1: Rdh54 mutants' effect interhomolog recombination

(A). Model of the Alphafold2 generated Rdh54 structure bound to dsDNA. The color scheme represents the pLDDT format colored structural model of yRdh54 in a closed conformation. Their AlphaFold2 per-residue confidence scores (pLDDT): very high confidence (pLDDT>90), dark blue; high confidence (90>pLDDT>70), cyan; low confidence (70>pLDDT>50), yellow; very low confidence (50>pLDDT), orange. DNA is shown in tan. The location of T851(magenta) and S852 (green) are indicated by dots. The predicted structure was obtained from uniprot, and the model was generated using PDB:1Z63 and PDB:3PJR.

(B). Assay designed to identify gene conversion between homologous chromosomes. The assay is dependent on the formation of an *LEU2* from two inactive *leu2* alleles.

(C). Comparison of inter-homolog gene conversion frequencies for WT, *rdh54T851A*, *rdh54T851D*, *rdh54S852A*, *rdh54S852D*, and *rdh54T851AS852A*. The crossbar represents the mean, and the error bars the standard deviation of at least three independent experiments from multiple crosses.

Figure 2

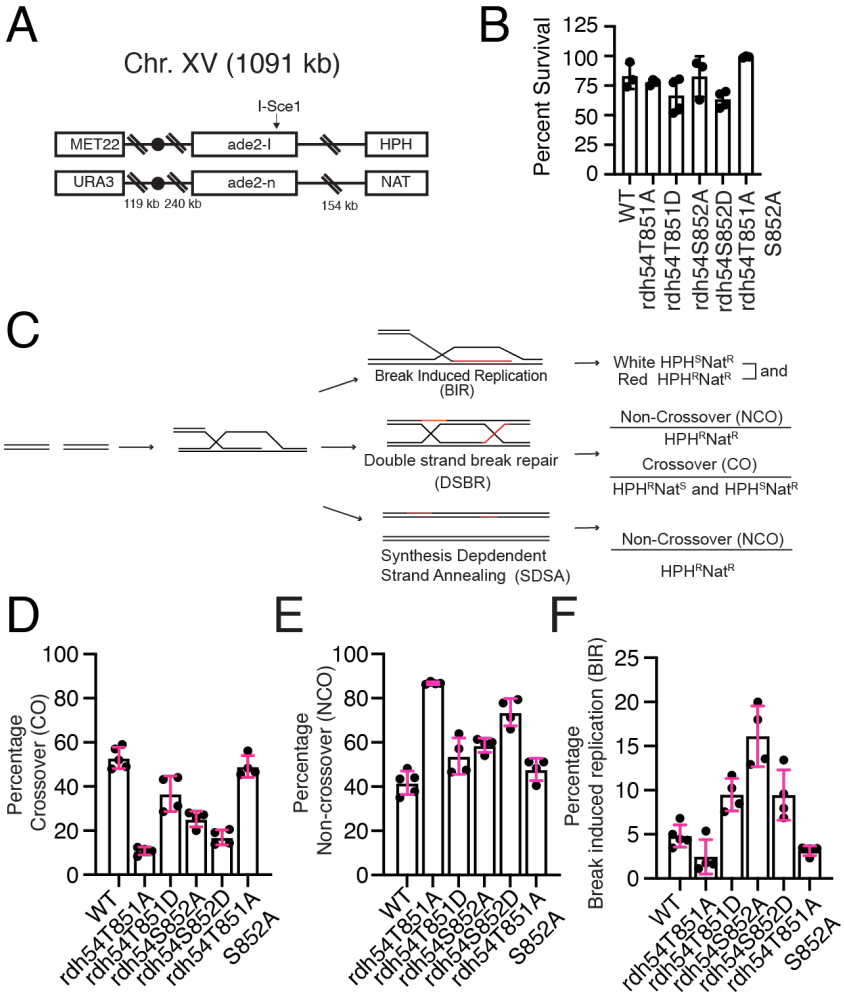

Figure 2: *rdh54T851A* has altered CO to NCO outcomes

(**A).** Schematic diagram illustrating the configuration of the HR reporter assay used in our study to monitor HR outcomes.

(B). Percentage survival of cells treated with and without galactose for WT, *rdh54T851A*, *rdh54T851D*, *rdh54S852A*, *rdh54S852D, rdh54T851A,S852A*. The bars represent the mean, and the error bars represent the standard deviation for at least three independent experiments.

(C). Schematic diagram illustrating the LOH outcomes that can be used to determine exchange between chromosomes.

(D). Percentage of HR outcomes that resulted in CO for WT, *rdh54T851A*, *rdh54T851D*, *rdh54S852A*, and *rdh54S852D, rdh54T851A,S852A*. The bars represent the mean, and the error bars represent the standard deviation for four independent experiments and crosses.

(**E).** Percentage of HR outcomes that resulted in NCO for WT, *rdh54T851A*, *rdh54T851D*, *rdh54S852A*, *rdh54S852D, and rdh54T851A,S852A*. The bars represent the mean, and the error bars represent the standard deviation for four independent experiments and crosses.

(F). Percentage of HR outcomes that resulted in BIR for WT, *rdh54T851A*, *rdh54T851D*, *rdh54S852A*, *rdh54S852D, and rdh54T851A,S852A*. The bars represent the mean, and the error bars represent the standard deviation for four independent experiments and crosses.

Table 1

RDH54 ALLELE	IH Gene Conversion ($x10^{-5}$)	CO percent (Fraction of WT)	NCO percent (Fraction of WT)	BIR percent (Fraction of WT)	Intrachromosomal Template Switching (ICTS) ($x10^{-5}$)
WT	1.0	54 (1.0)	41.1 (1.0)	4.9 (1.0)	16.27 (1.0)
RDH54Δ	0.92	N/A	N/A	N/A	N/A
T851A	0.35	10.6 (0.19)	87 (2.1)	2.4 (0.5)	7.3 (0.44)
T851D	0.9	36.9 (0.68)	53.7 (1.3)	9.4 (1.8)	13.7 (0.84)
S852A	0.45	25.5 (0.47)	58.5 (1.4)	16 (3.2)	14.93 (0.91)
S852D	0.88	17 (0.31)	73.6 (1.8)	9.4 (1.8)	10.27 (0.63)
T851AS852A	1.0	49.2 (0.91)	47.7 (1.1)	3.1 (0.62)	11.83 (0.72)

Table 1: Summary of genetic data for phosphomimic and alanine mutations in Rdh54
IH, interhomolog; CO, crossover; NCO, non-crossover; BIR, break-induced replication; ICTS, intrachromosomal template switching.

Figure 3

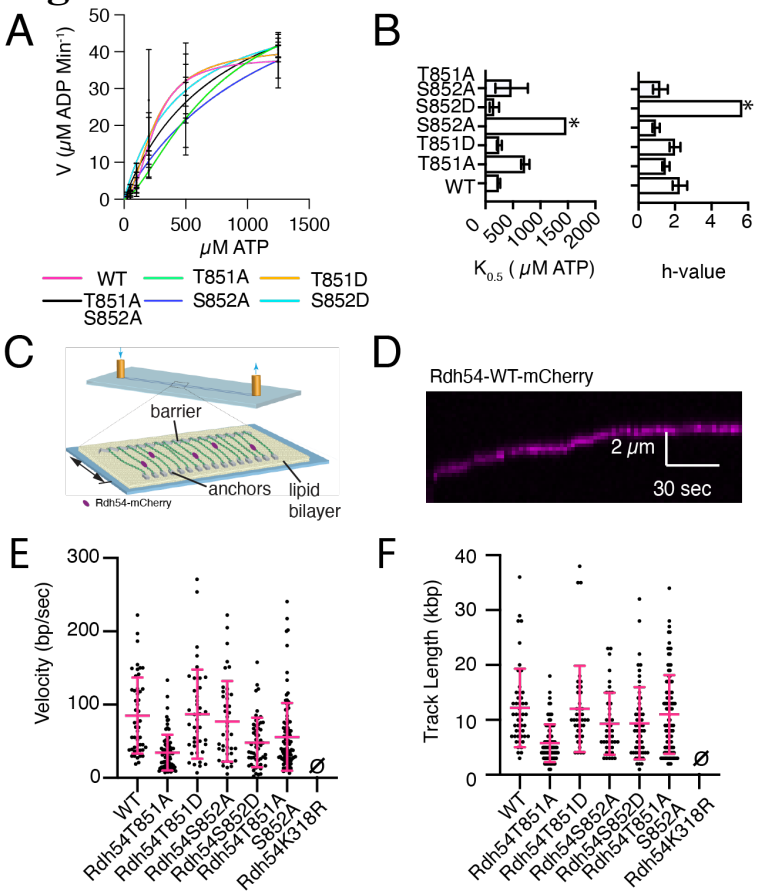

Figure 3: Mutations in Rdh54 result in slowed translocation on dsDNA

(A). ATP hydrolysis rates for Rdh54, Rdh54T851A, Rdh54T851D, Rdh54S852A, Rdh54S852D, and Rdh54T851AS852A. All data are fit by an allosteric model. The error bars represent the standard deviation of at least four independent experiments.

(B). Bar graph illustrating the $K_{0.5}$ values (left) and h-values (right) for Rdh54, Rdh54T851A, Rdh54T851D, Rdh54S852A, Rdh54S852D, and Rdh54T851AS852A. The error bars represent the confidence interval in the fit of the data. * Denotes fits of low confidence which lack error bars and should be considered qualitative

(C). Schematic diagram illustrating DNA curtains setup, a single molecule approach that allows measurement of Rdh54-mCherry velocity and track length.

(D). Representative kymograph illustrating the translocation of Rdh54-mCherry along dsDNA.

(E). Translocation velocities (bp/sec) for individual translocation events of Rdh54 (N=48), Rdh54T851A (N=81), Rdh54T851D (N=40), Rdh54S852A (N=42), Rdh54S852D (N=56), and Rdh54T851AS852A (N=101). The crossbar represents the mean of the data, and the error bar represents the standard deviation of the experiment.

(F). Track lengths (kbp) for individual translocation events of Rdh54 (N=48), Rdh54T851A (N=81), Rdh54T851D (N=40), Rdh54S852A (N=42), Rdh54S852D (N=56), and Rdh54T851AS852A (N=101). The crossbar represents the mean of the data, and the error bars represent the standard deviation of the experiments.

Figure 4

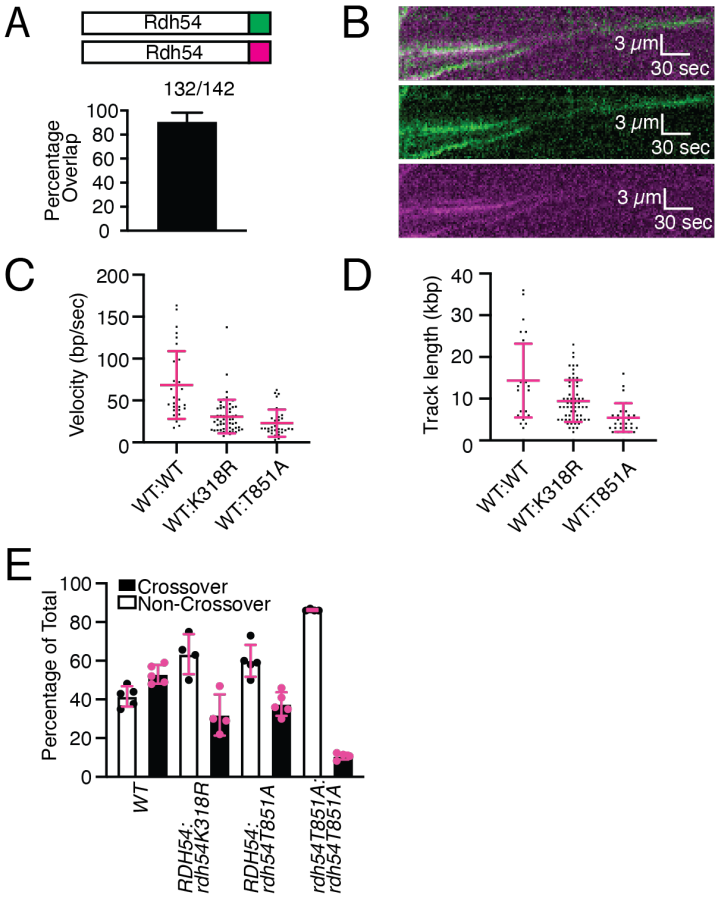

Figure 4: Rdh54 forms a mixed oligomer during translocation

(A). Schematic illustrating experiments performed with equal molar Rdh54-mCherry and Rdh54-GFP (Top). Graphical representation of the number of Rdh54-mCherry molecules that overlap with Rdh54-GFP molecules. The error bar represents the standard deviation of three independent experiments (Bottom).

(B). Representative kymographs illustrating the co-translocation of Rdh54-mCherry and Rdh54-GFP molecules. The channels are merged (top), magenta (middle), and green (bottom). **(C).** Dot plot representing the velocities (bp/sec) of mixed WT:WT (1:1) (N=32), WT:Rdh54K318R (1:1) (N=62), and WT-Rdh54T851A (1:1) (N=31). The bar and the error bars represent the mean and standard deviation of the data.

(D). Dot plot of the track lengths (kbp) of mixed WT:WT (1:1) (N=32), WT:Rdh54K318R (1:1) (N=62), and WT-Rdh54T851A (1:1) (N=31). The bar and the error bars represent the mean and standard deviation of the data.

(E). Percentage of CO and NCO outcomes for WT, *RDH54:rdh54K318R*, and *RDH54:rdh54T851A* strains. The bar represents the mean, and the error bars represent the standard deviation of four independent experiments from four different zygotes.

Figure 5

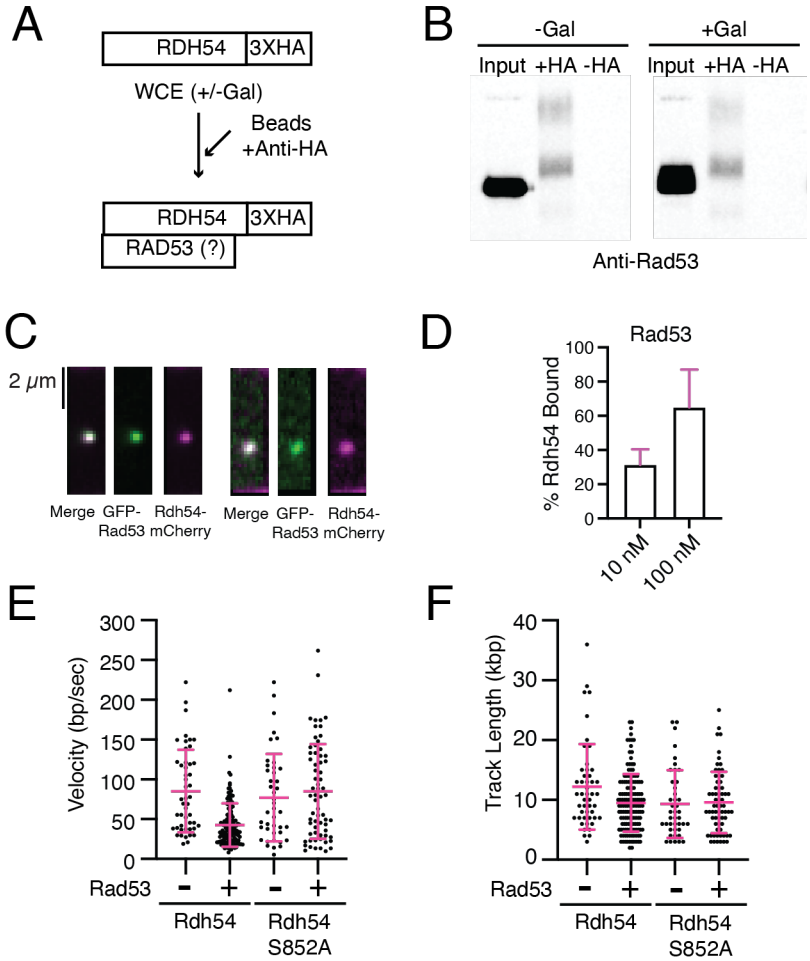

Figure 5: Rad53 directly regulates Rdh54 activity

(A). Schematic illustrating the experiment to use a Rdh54-HA strain to test for an interaction between Rad53 and Rdh54.

(B). Representative western blot illustrating the co-immunoprecipitation of Rad53 with Rdh54.

(C). Two individual dsDNA molecules bound by Rdh54 (Magenta) and Rad53 (Green).

(D). Bar graph representing the percentage of Rdh54 bound by Rad53 at 10 nM and 100 nM. The error bars represent the standard deviation of at least three independent experiments.

(E). Translocation velocities (bp/sec) for WT-Rdh54 with (N=142) and without (N=48) Rad53 treatment and Rdh54S852A with (N=66) and without (N=42) Rad53. The WT-Rad53 and the Rdh54S852A-Rad53 are reproduced from Figure 3.

(F). Track lengths (kbp) for WT-Rdh54 with (N=142) and without (N=48) Rad53 treatment and Rdh54S852A with (N=66) and without (N=42) Rad53 treatment. The WT-Rad53 and the Rdh54S852A-Rad53 are reproduced from Figure 3.

Figure 6

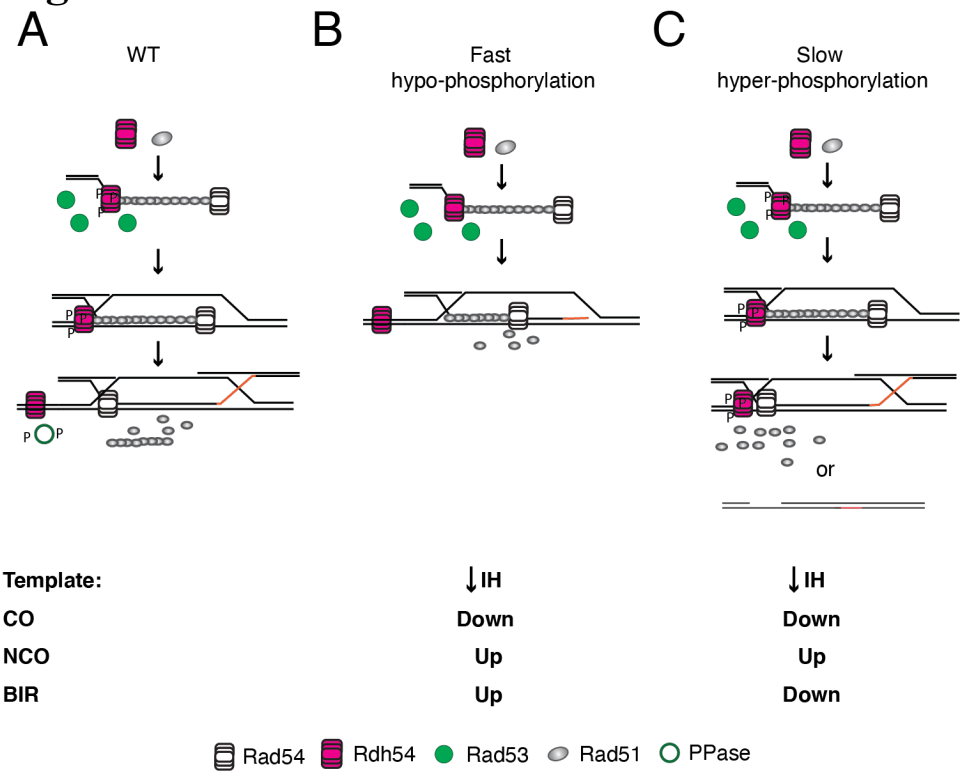

Template:	↓IH	↓IH
CO	Down	Down
NCO	Up	Up
BIR	Up	Down

Figure 6: Kinetic regulation of HR outcomes by Rdh54 phosphorylation.
(A). Hypothetical model for how Rdh54 may stabilize early HR intermediates. In this model Rdh54 is phosphorylated by Rad53 which stabilizes HR intermediates involved in target selection or second end capture.
(B). Rdh54 molecules that are not phosphorylated move quickly away from HR intermediates leading to their premature destabilization reducing second end capture.
(C). Rdh54 molecules that are slow moving, or hyperphosphorylated, lead to overstabilization of intermediates and increases in NCO outcomes that may occur through SDSA or NCO resolution of dHJs.

Extended Data Table 1

Strains	Genotype	Source or reference
LSY-2202-15D (WT)	*MATta ade2-n his3::NatMX4 met22:klURA3*	*(Mazon et al. 2010)*
LSY-2205-11C (WT)	*MATalpha ade2-I lys2:GAL-ISCE1 his3:HphMX4*	*(Mazon et al. 2010)*
JBC0011 (15D)	*RDH54::RDH54-KanMX*	*(Keymakh et al. 2022)*
JBC0013 (11C)	*RDH54::RDH54-KanMX*	*(Keymakh et al. 2022)*
JBC0014 (15D)	*RDH54::rdh54K318R*	*(Keymakh et al. 2022)*
JBC0016 (11C)	*RDH54::rdh54K318R*	*(Keymakh et al. 2022)*
JBC0018 (15D)	*RDH54::rdh54T851A*	*This study*
JBC0020 (11C)	*RDH54::rdh54T851A*	*This study*
JBC0026 (15D)	*RDH54::rdh54S852A*	*This study*
JBC0028 (11C)	*RDH54::rdh54S852A*	*This study*
JBC0054 (15D)	*RDH54::rdh54S852D*	*This study*
JBC0060 (11C)	*RDH54::rdh54S852D*	*This study*
JBC0056 (15D)	*RDH54::rdh54T851D*	*This study*
JBC0062(11C)	*RDH54::rdh54T851D*	*This study*
JBC0086 (15D)	*RDH54::rdh54T851AS852A*	*This study*
JBC0092 (11C)	*RDH54::rdh54T851AS852A*	*This study*
BY4741 (WT)		*Dharmacon*
BY4741	*rdh54Δ*	*Dharmacon*
HK663A-leu2-R1 (A)	*leu2-Ecor1 RAD5+ ade2-1 can1-100 his3-11,15 trp1-1 ura3*	*(Klein H 1997)*
HK6793B-leu2BSTEII (alpha)	*leu2-BstEII RAD5+ ade2-1 can1-100 his3-11,15 trp1-1 ura3*	*(Klein H 1997)*
JBC206	*leu2-Ecor1 RAD5+ ade2-1 can1-100 his3-11,15 trp1-1::TRP1 ura3*	*This study*
JBC207	*leu2-BstEII RAD5+ ade2-1 can1-100 his3-11,15 trp1-1 ura3::URA3*	*This study*
JBC0174	*JBC206 RDH54::RDH54-KanMX*	*This study*
JBC0175	*JBC206 RDH54::rdh54T851A-KanMX*	*This study*
JBC0176	*JBC206 RDH54::rdh54T851D-KanMX*	*This study*
JBC0177	*JBC206 RDH54::rdh54S852A-KanMX*	*This study*
JBC178	*JBC206 RDH54::S852D-KanMX*	*This study*
JBC179	*JBC206 RDH54::rdh54T851AS852A-KanMX*	*This study*
JBC0180	*JBC207 RDH54::RDH54-KanMX*	*This study*
JBC0181	*JBC207 RDH54::rdh54T851A-KanMX*	*This study*

JBC0182	*JBC207 RDH54::rdh54T851D-KanMX*	*This study*
JBC0183	*JBC207 RDH54::rdh54S852A-KanMX*	*This study*
JBC0184	*JBC207 RDH54::S852D-KanMX*	*This study*
JBC0185	*JBC207 RDH54::rdh54T851AS852A-KanMX*	*This study*
yRA53	Mata::DEL Hocs::hisG uraD851trp1DEL63 leu2::KAN hmlDEL::hisGHMR::ADE3 ade3::GAL::Hocan1DEL::UR::Hocs::NAT, RA::LEU2, A3::TRP1	*Anand et al 2014*
JBC0084	*yRA53 leu2::KAN::HPHMX*	*This study*
JBC0099	*JBC0084 RDH54::RDH54KanMX*	*This study*
JBC0100	*JBC0084 RDH54::rdh54T851A*	*This study*
JBC0101	*JBC0084 RDH54::rdh54T851D*	*This study*
JBC0102	*JBC0084 RDH54::rdh54S852A*	*This study*
JBC0103	*JBC0084 RDH54::rdh54S852D*	*This study*
JBC0162	*JBC0084 RDH54::rdh54T851AS852A*	*This study*
JKM179	*hoΔ hml::ADE1 MATα hmr::ADE1 ade1-110 leu2,3-112 lys5 trp1::hisG ura3-52 ade3::GAL:HO*	*Kind gift from J. Haber*
JBC0144	*JKM179 RDH54::RDH54-3xHA-KanMX*	*This study*
Diploid (JBC0011 X JBC0013)	*RDH54::RDH54-KanMX/ RDH54::RDH54-KanMX*	*This study*
Diploid (JBC0011XJBC0016)	*RDH54::RDH54-KanMX /RDH54::rdh54K318R*	*This study*
Diploid (JBC0011XJBC0020)	*RDH54::RDH54-KanMX/ RDH54::rdh54T851A*	*This study*
Diploid (JBC0018XJBC0020)	*RDH54::rdh54T851A/ RDH54::rdh54T851A*	*This study*
Diploid (JBC0026X0028)	*RDH54::rdh54S852A/ RDH54::rdh54S852A*	*This study*
Diploid(JBC0054XJBC0060)	*RDH54::rdh54S852D/ RDH54::rdh54S852D*	*This study*
Diploid(JBC0056XJBC0062)	*RDH54::rdh54T851D/RDH54::rdh54T851D*	*This study*
Diploid (JBC0086XJBC0092)	*RDH54::rdh54T851AS852A/RDH54::rdh54T851AS852A*	*This study*
Diploid (JBC174XJBC180)	*RDH54::RDH54-KanMX/ RDH54::RDH54-KanMX*	*This study*
Diploid(JBC175XJBC181)	*RDH54::rdh54T851A/ RDH54::rdh54T851A*	*This study*
Diploid(JBC176XJBC182)	*RDH54::rdh54T851D/RDH54::rdh54T851D*	*This study*
Diploid(JBC177XJBC183)	*RDH54::rdh54S852A/ RDH54::rdh54S852A*	*This study*
Diploid (JBC178XJBC184)	*RDH54::rdh54S852D/ RDH54::rdh54S852D*	*This study*
Diploid (JBC179XJBC185)	*RDH54::rdh54T851AS852A/RDH54::rdh54T851AS852A*	*This study*

Extended Data Table 2

Plasmid backbone	Construct	Source
pET15	6xHis-Rdh54-WT	**This study**
pET15	6xHis-Rdh54K318R	**This study**
pET15	6xHis-Rdh54T851A	**This study**
pET15	6XHis-Rdh54T851D	**This study**
pET15	6xHis-Rdh54S852A	**This study**
pET15	6xHis-Rdh54S852D	**This study**
pET15	6xHis-Rdh54T851AS852A	**This study**
pET15	6xHis-Rdh54-mCherry-WT	**This study**
pET15	6xHis-Rdh54-mCherryK318R	**This study**
pET15	6xHis-Rdh54-mCherryT851A	**This study**
pET15	6xHis-Rdh54-mCherryS852A	**This study**
pET15	6xHis-Rdh54-mCherryT851D	**This study**
pET15	6xHis-Rdh54-mCherryS852D	**This study**
pET15	6xHis-Rdh54-mCherryT851AS852A	**This study**
pRS415	*RDH54-WT*	**This study**
pRS415	*rdh54S21A*	**This study**
pRS415	*rdh54S167A*	**This study**
pRS415	*rdh54S387A*	**This study**
pRS415	*rdh54S621A*	**This study**
pRS415	*rdh54S790A*	**This study**
pRS415	*rdh54S791A*	**This study**
pRS415	*rdh54T851A*	**This study**
pRS415	*rdh54S852A*	**This study**
pRS415	*rdh54K318R*	**This study**
pRS415	*rdh54K318RT851A*	**This study**
pRS305	*RDH54-KanMX*	**This study**
pRS305	*rdh54T851A-KanMX*	**This study**
pRS305	*rdh54T851D-KanMX*	**This study**
pRS305	*rdh54S852A-KanMX*	**This study**
pRS305	*rdh54S852D-KanMX*	**This study**
pRS305	*rdh54K318R-KanMX*	**This study**
pRS305	*rdh54T851AS852A-KanMX*	**This study**
pET15	6xHis-Rad53	**A kind gift from Dirk Remus**
pET15	6xHis-GFP-Rad53	**This study**

Extended Data Table 3

Strain	CO	NCO	BIR	Total	Chromosome Loss
WT	94	72	8	174	0
rdh54T851A:rdh54T851A	76	611	17	704	0
rdh54T851D:rdh54T851D	122	189	32	343	0
rdh54S852A:rdh54S852A	42	93	25	160	0
rdh54S852D:rdh54S852D	74	343	31	448	1
RDH54:rdh54T851A	64	125	7	196	0
RDH54:rdh54K318R	62	125	9	183	0
rdh54T851AS852A:rdh54T851AS852A	186	181	12	379	0

Extended Data Figure 1

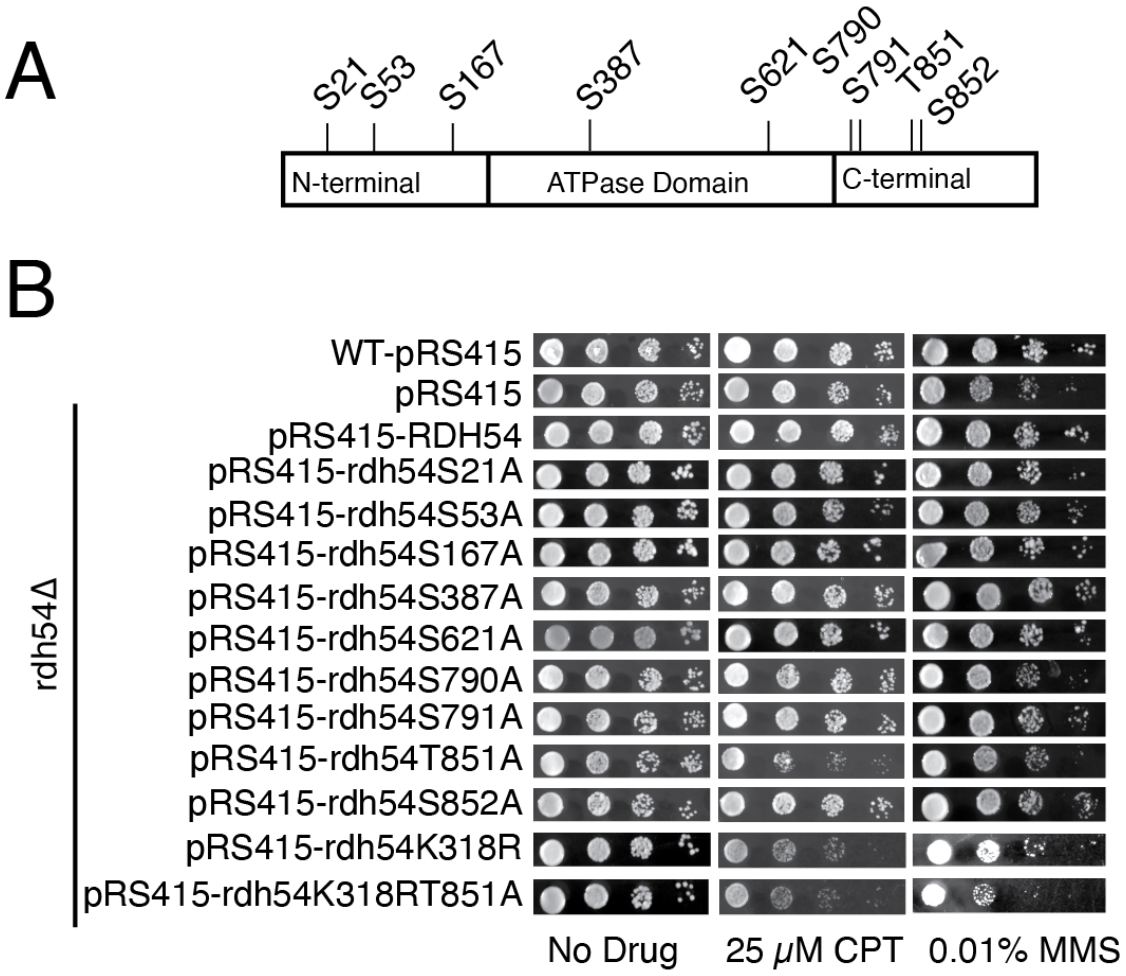

Supplemental Figure 1: *rdh54T851A* shows enhanced DNA damage phenotype
(A). Schematic diagram illustrating Rdh54 phosphosites as identified by the database SuperPhos. All S/T were converted to A.
(**B).** Yeast growth assays to measure the growth of different *RDH54* alleles in the presence of 25 μM CPT or 0.01% MMS.

Extended Data Figure 2

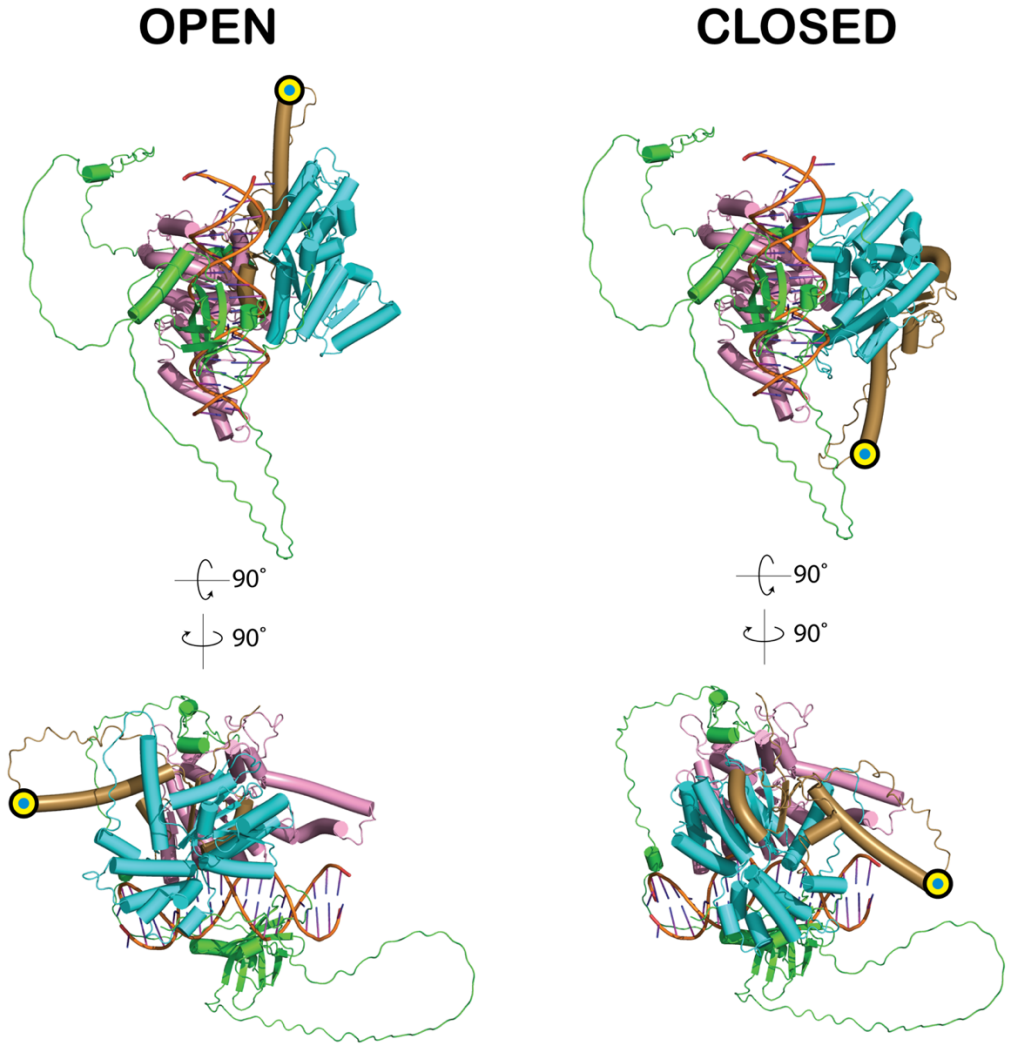

Supplemental Figure 2: Additional views of the open and closed models of yRdh54. To generate the open and closed models of yRdh54, the two RecA-like domains in the AlphaFold predicted structure of yRdh54 (https://www.uniprot.org/uniprotkb/B3LN76) were individually superimposed onto the equivalent domains of either the *Sulfalobus solfataricus* SWI2/SNF2 ATPase in the DNA-bound open state (PDB:1Z63), or AMP-PNP:DNA bound PcrA (PDB:3PJR) in the closed state. Most of the N-terminal domain of yRdh54 (green, residues: 1-261) is predicted to be unstructured (per-residue confidence (pLDDT) score < 50) and its position relative to other parts of the model cannot be interpreted. Lobe 1 (residues: 262-259), pink; lobe 2 (residues: 550-807), cyan; C-terminal domain (residues: 808-924), brown. The position of T851 is indicated with a yellow and cyan bullseye. DNA coordinates (orange) are from the *S. solfataricus* ATPase X-ray crystal structure (PDB:1Z63).

Extended Data Figure 3

A

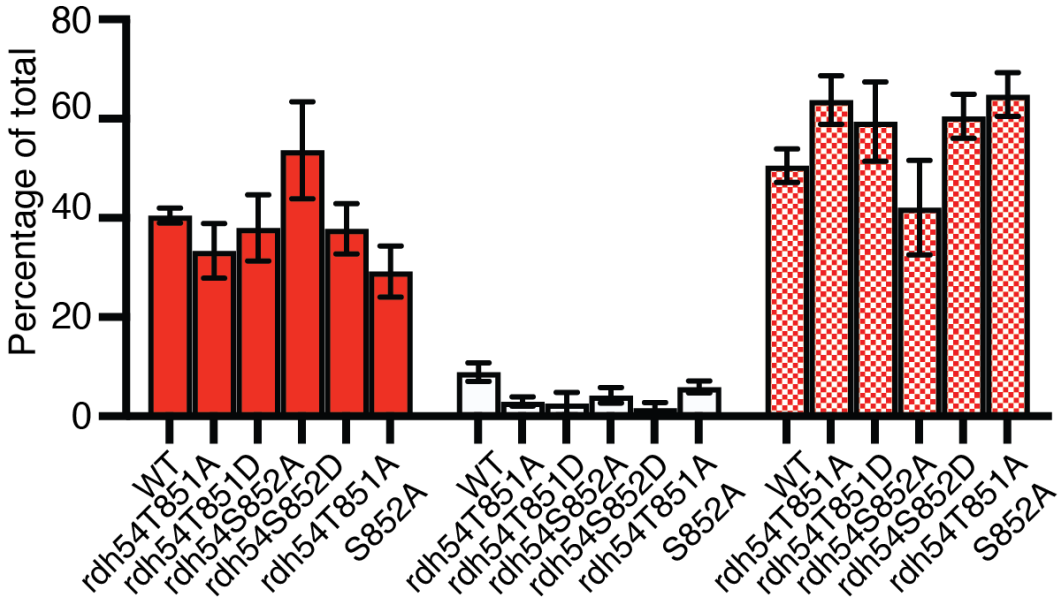

Supplemental Figure 3: *RDH54* mutants to not alter long tract versus short tract gene conversion

(A). Percentage of red, white, and sectored colonies for each *RDH54* mutant. The bar represents the mean, and the error bars represent the standard deviation of four independent experiments.

Extended Data Figure 4

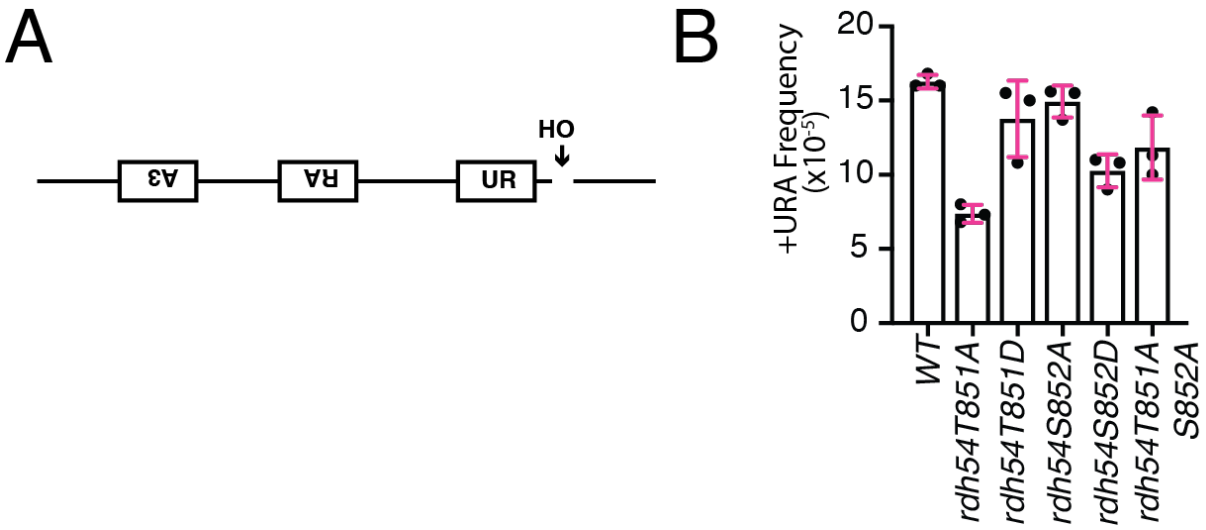

Supplemental Figure 4: *RDH54* mutants are also defective in DNA template switching
(A). Template defining assay used to measure intrachromosomal template switching during DSBR. The completion of an intact *URA3* gene requires a template switch to occur during repair.
(B). Measured *Ura+* frequency for *RDH54* WT and different phosphomimic alleles of *RDH54*. The bar represents the mean, and the error bars represent the standard deviation for three independent experiments.

Extended Data Figure 5

A

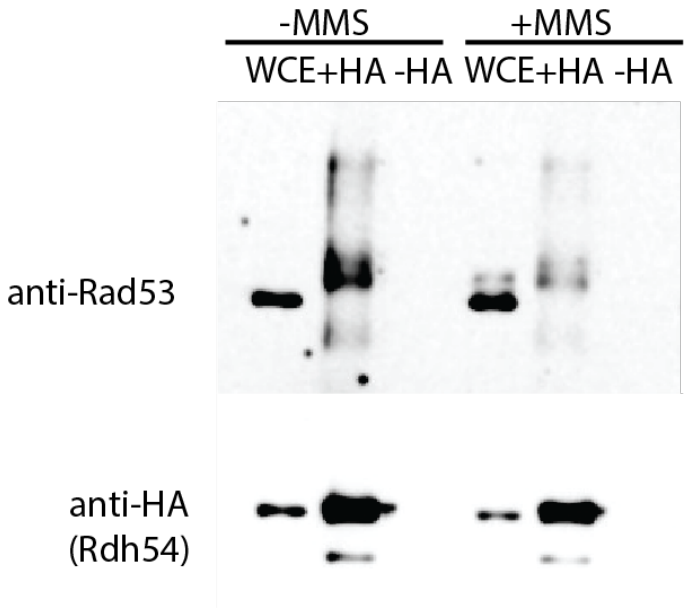

Supplemental Figure 5: Rdh54 and Rad53 interact in the absence of DNA damage.
(A). Representative western blot demonstrating a co-IP of Rad53 with Rdh54. The top blot is probed with an anti-Rad53 antibody, and the bottom is probed with an anti-HA antibody.

Extended Data Figure 6

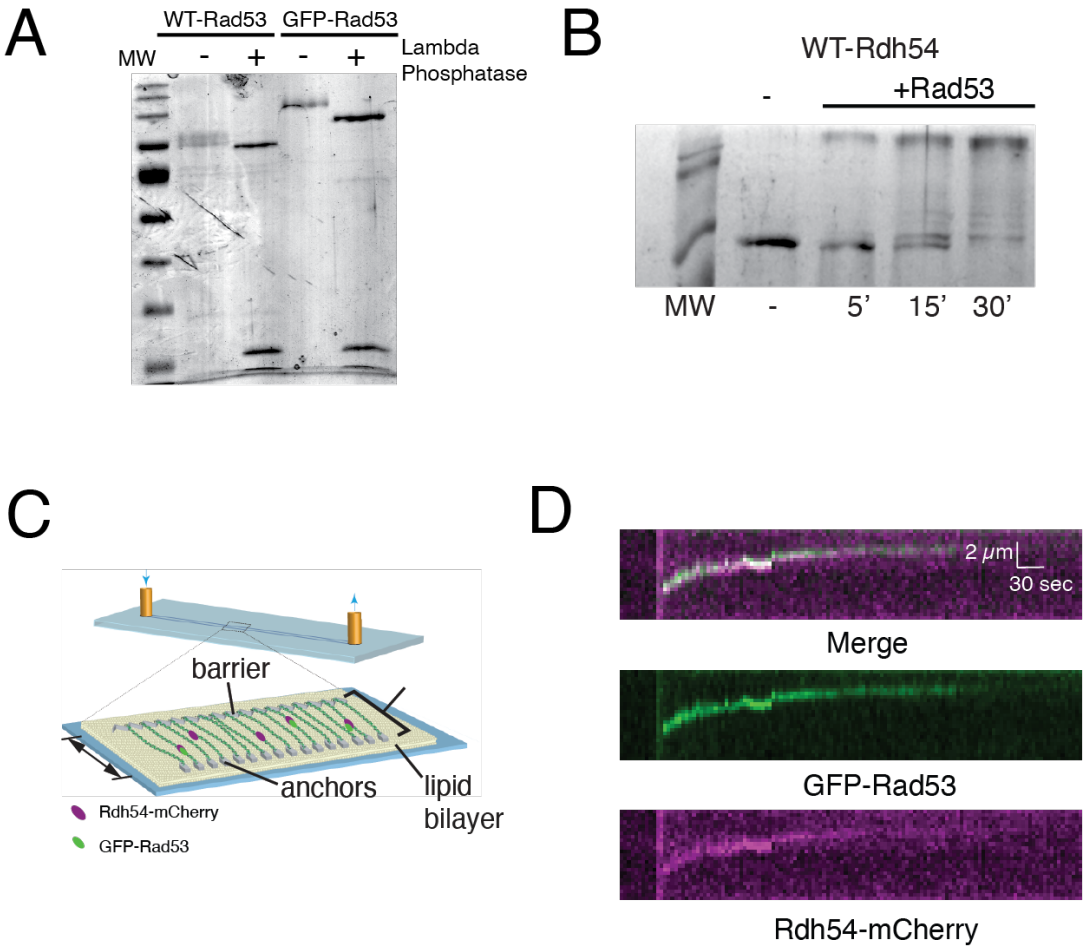

Supplemental Figure 6: Rdh54 directly interacts with and is a target of Rad53
(A). Representative SDS-PAGE illustrating purified Rad53 and GFP-Rad53 with and without Lambda phosphatase illustrating that Rad53 and GFP-Rad53 are purified in their phosphorylated form.
(B). SDS-PAGE phostag gel with un-phosphorylated Rdh54, and Rdh54 phosphorylated by Rad53 for 5', 15', and 30'.
(C). Schematic diagram illustrating DNA curtains experiment to measure the direct interaction between Rdh54-mCherry and GFP-Rad53.
(D). Representative kymograph illustrating the interaction between Rdh54-mCherry and GFP-Rad53. The Rdh54 molecule in this image is translocating along dsDNA.